NTNU

Norwegian University of
Science and Technology

Thermo-Hydro-Mechanical simulations of artificial ground freezing

Lorenzo Cicchetti

Cold Climate Engineering
Submission date: June 2018
Supervisor: Gustav Grimstad, IBM
Co-supervisor: Thomas Ingeman-Nielsen, DTU
Seyed Ali Ghoreishian Amiri, IBM

Norwegian University of Science and Technology
Department of Civil and Environmental Engineering

NTNU – Trondheim
Norwegian University of
Science and Technology

DTU Technical
University of
Denmark

Thermo-hydro-mechanical simulations of artificial ground freezing

Lorenzo Cicchetti

Cold Climate
Engineering

Nordic Master in Cold Climate Engineering

Submission date: 8 th June 2018

NTNU supervisor: Gustav Grimstad, Professor
NTNU co-supervisor: Seyed Ali Ghoreishian Amiri, Researcher
DTU supervisor: Thomas Ingeman-Nielsen, Associate Professor

Departments of Civil and Environmental Engineering at NTNU and DTU

Preface

The work presented here is a part of my joint MSc degree in Cold Climate Engineering, carried out at the Geotechnical Division of the Norwegian University of Science and Technology (NTNU) in the spring semester of 2018. The thesis is worth 30 ECTS and it is conducted in collaboration with the Techcnical University of Denmark (DTU). The main supervisor at NTNU was Prof. Gustav Grimstad, with co-supervision of Dr. Seyed Ali Ghoreishian Amiri. DTU supervisor was Prof. Thomas Ingeman-Nielsen at the department of Civil and Environmental Engineering. The idea of studying Thermo-Hydro-Mechanical simulations of artificial ground freezing was born during a constructive discussion with Professors Steinar Nordal and Gustav Grimstad with regard to geotechnical aspects of frozen soils at the beginning of the autumn semester of 2017. Part of the literature review here presented was performed for the course TBA4510 - Specialization Project on Artificial Ground Freezing. In addition, preliminary results of this MSc thesis have been presented in a poster at the ARTEK International Conference on Transportation Infrastructure Engineering in Cold Regions held in Sisimiut, Greenland on May 1st. The poster has been awarded the best student poster of the conference by the evaluating scientific committee.

Trondheim, June 2018

Lorenzo Cicchetti

This page is intentionally left blank

Acknowledgment

Firstly, I would like to express my very profound gratitude to my daily supervisor and mentor at NTNU, Dr. Seyed Ali Ghoreishian Amiri for his patient guidance, knowledge, and enthusiasm that he has provided me throughout my time as his student. He was always willing to help and encourage me, even when the model did not seem to work. He also assisted me in writing the manuscript and preparing the poster for the ARTEK International Conference in Greenland. This MSc thesis would not have come together without his commitment and technical support.

I would also like to thank my two other supervisors: Prof. Gustav Grimstad at NTNU for supporting and guiding me since the autumn semester and Prof. Thomas Ingeman-Nielsen at DTU for the academic expertise he provided during the Arctic Semester in Greenland. Their presence and their encouragement before the poster presentation at the ARTEK International Conference were reassuring and very important for me.

Next, my sincere thanks go to my best friends Francesco, Chiara and Malvina which have always been by my side and especially to my girlfriend Angelica for providing me with unfailing and continuous encouragement throughout my years of study abroad and during the development of this MSc thesis. This accomplishment would not have been possible without you.

Finally, I must express my very profound gratitude to my parents Augusto e Claudia, my sister Chiara, my brother Luca and all my relatives. Their inspirational and heartening words gave me the energy and motivation to pursue the goal and accomplish this major step in my life. Thank you.

L.C.

This page is intentionally left blank

Abstract

Hundreds of thousands of people in Alaska, Canada, Russia and Greenland live on permafrost, which covers nearly 24% of the northern hemisphere (National Snow and Ice Data Center, 2018). Living conditions can be challenged by the fragile nature of the frozen ground, especially if framed in the context of global warming. Indeed, permafrost effects like frost heave and thaw settlement may heavily affect existing buildings and transportation infrastructure such as roads, railways, embankments and runways. These being vital for isolated Arctic communities, should be preserved and maintained. Artificial Ground Freezing (AGF) can be employed to keep soil frozen and hence ensure structure stability by means of one-way heat pipe systems, also called thermosyphons. Such devices have been widely used in China where permafrost degradation of the Tibet plateau posed severe threats to the normal functioning of the Qinghai-Tibet railway (Mu et al., 2016b). Also Greenlandic infrastructure system is facing the same problems. The airport and many buildings in the settlement of Kangerlussuaq are for example threatened by the shifting thermal regime of the underneath soil and are in need of maintenance. Artificial ground freezing is also used nowadays as a valuable and efficient construction method for underground engineering projects in densely urbanized areas, due to the enhanced soil strength and decreased permeability it provides. This technique allows forming earth support systems covering a variety of geotechnical problems such as structural underpinning for foundation improvement, tunnel constructions and temporary control of groundwater flow in construction processes. A good example is the construction of Naples underground in Italy, where artificial ground freezing has been successfully applied. Thus, it seems clear that the interest in frozen ground engineering, whether soil freezing is induced by natural conditions or by human activities, has rapidly developed over the last decades and it is expected to continue growing.
To predict the coupled thermo-hydro-mechanical (THM) behaviour of frozen soil and to provide a reliable design tool for geotechnical engineers, the development of a numerical modeling approach is necessary. To this purpose, Ghoreishian Amiri et al. (2016b) developed a new constitutive THM model able to capture different behaviors of frozen soil and predict mechanical response under different loading conditions and variations of temperature. This model will be used in this MSc thesis to replicate monitoring results of a large-scale artificial ground freezing project, that is the construction of platform tunnels in Naples Underground. This aims to further validate the robustness and the correct theoretical implementation of the model, when applied to more advanced case studies.

Contents

List of Figures

List of Tables

Chapter 1

Introduction

1.1 Background and motivation

Frozen ground engineering has undergone a rapid development in the last decades. Due to the increase in engineering activities in cold regions, soil freezing and thawing processes have become a hot research topic among scientists and geotechnical engineers. Change in soil thermal regime and the subsequent landscape reshaping can negatively affect the performance of structures, which may be subjected to uneven heave and settlements. In a global warming context, besides the associated increase in the vulnerability of infrastructure due to permafrost degradation, also geocryological hazards turned out to be a serious threat to the normal functioning of Arctic communities and to their economic development (Streletskiy et al., 2012).
Additionally, an increase in the use of artificial ground freezing is expected in the upcoming years. Many underground projects in densely built-up areas of more temperate regions have indeed made use of this technique in order to temporarily increase soil strength while drastically decreasing its permeability. Here, the main challenges lie in preserving the integrity of the surrounding buildings, limiting to the greatest possible extent any vertical displacement of soil. It becomes therefore extremely important to understand the mechanical behaviour of frozen ground under different loading and temperature conditions in order to develop and provide a reliable numerical modeling approach.

1.2 Living on frozen ground

Hundreds of thousands of people in Alaska, Canada, Russia and Greenland live on permafrost and their lifestyle and livelihood is highly affected by frozen ground (National Snow and Ice Data Center, 2018). Buildings built on permafrost are heated from the inside and a bad insulation often allows heat to be given off and thaw the frozen ground underneath. In addition, the ongoing global warming is accelerating the permafrost thawing rate up to 0.04 m/yr in Alaska since 1992 (Solomon et al., 2007). Romanovsky et al. (2017) also report that the average active layer thickness (ATL) has increased significantly in the cold regions, primarily in the Siberian Arctic. This thermal degradation of frozen ground can result in uneven foundation settling and serious consequences for buildings, as shown in Figure 1.1:

Figure 1.1: Building in Ilulissat (Greenland) visibly deformed due to thawing permafrost

Special attention as well as a careful design entail the correct choice of foundation type and insulation method, which acquire a fundamental importance in this context. Not only buildings, but also transportation infrastructure are strongly affected by differential heave and settlements and constant maintenance is needed to keep them operative and safe (Ingeman-Nielsen, 2017).

Permafrost degradation can lead to extensive damages as observable from Figure 1.2, which shows a depression formation and pavement cracking at the Greenlandic airport of Kangerlussuaq. Here, a surveying campaign performed by DTU students in May 2017 as part of the course "11854 - Infrastructure construction in the Arctic" revealed that local thaw settlements are still active in that part of the runway which extends on top of fine-grained and very ice-rich marine sediments. Infrastructure and buildings that are currently not resting on bedrock will experience an increasing occurrence of uneven settling and potential degradation, exacerbated by warming conditions. Daanen et al. (2011) state that construction and maintenance costs in Greenland are expected to increase dramatically if current practices are not adapted to increasing temperature and permafrost degradation. Economic considerations made by Andersland and Ladanyi (2004) depict that frost action is the major cause of damage to buildings and transportation infrastructure in all Arctic regions and according to DiMillio (1995) over two billion dollars are spent annually only in the United States to repair and improve the riding quality of traffic surfaces. The next subsections deals with engineering considerations about frost action, defined as the detrimental process of frost heave during freezing periods followed by thaw weakening and decrease of bearing capacity upon thawing.

Figure 1.2: Thaw settlements and cracking at Kangerlussuaq airport in May 2017

1.2.1 Frost heave

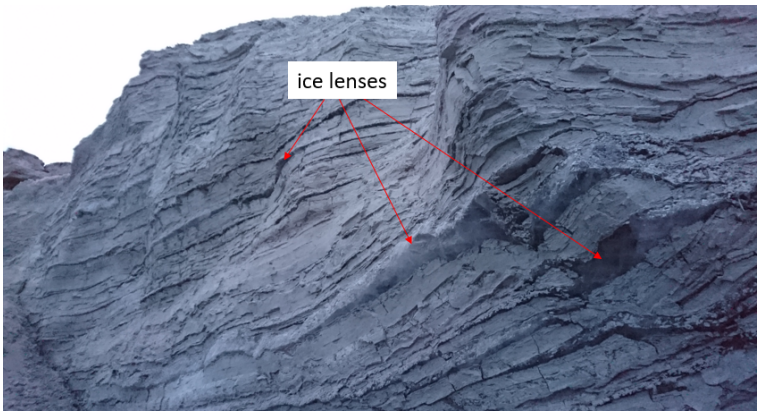

Figure 1.3: Ice lenses in permafrost along the river bank in Kangerlussuaq in May 2017

The term frost heave refers to the swelling of soil due to ice segregation into a series of lenses, which can be observed in Figure 1.3. Formation of ice lenses is triggered by capillary rise of water which meets the freezing front. Volumetric expansion of water due to phase change leads to the increment of pore pressure within the unfrozen pores and the development of a cryogenic suction gradient at the ice-water interface, responsible for drawing pore water in the unfrozen soil towards the freezing front (Thomas et al., 2009). Greater heave can manifest as a consequence of slow freezing processes in which there is more time for water to migrate. The velocity with which water is transported is not only dependent on the developed pressure deficiency but also on the unfrozen soil permeability, as predicted by Darcy's law (Andersland and Ladanyi, 2004). This explains the non-frost susceptibility of coarse soils with respect to finer grained materials like silts or clays in which, however, the unfrozen zone may desiccate due to water being driven towards the freezing front faster than it can be provided by the water table (Jones, 1996). The sequence of events related to frost heave development is depicted in Figure 1.4, which shows a homogeneous fine-grained soil column subject to one-sided natural freezing from top down:

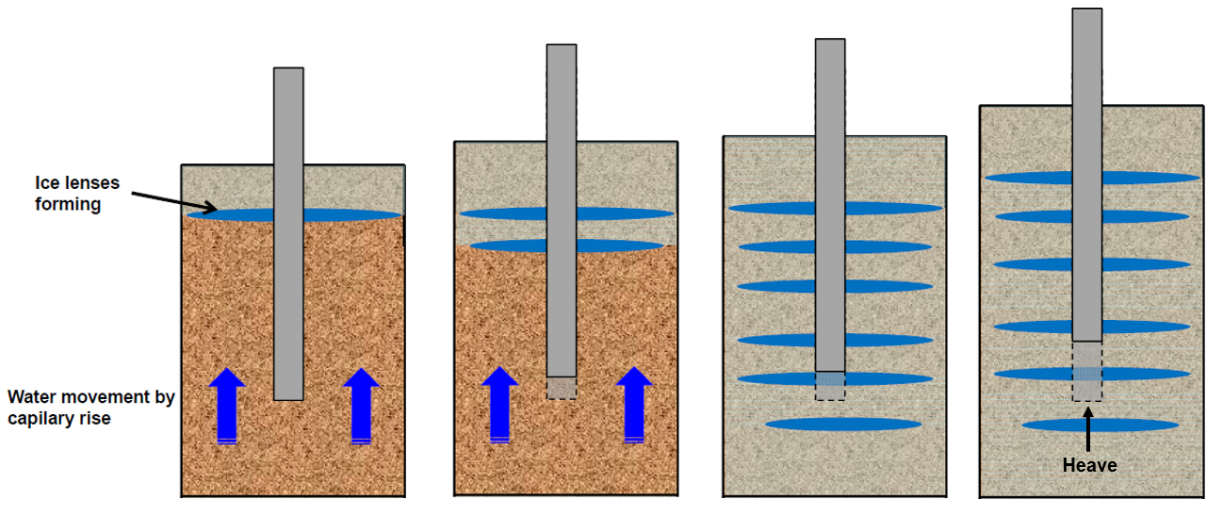

Figure 1.4: Schematic of ice lens formation and frost heave development. Water migration from lower and unfrozen regions deposits as bands of pure ice, forcing the soil apart as they grow and thus heaving the surface upwards (Ingeman-Nielsen, 2017)

When frozen soil swelling is hindered by existing building foundations, a significant heaving pressure may develop, and uplift forces are transmitted to the foundations from different directions (Andersland and Ladanyi, 2004). Whereas uniform heave movements would be tolerated by many buildings, soil heterogeneity causes differential movements in the ground which are detrimental to the overall stability of structures.

Frost susceptibility of soils

Soils which result particularly sensitive to frost heave are known as frost-susceptible. The U.S. Army Coprs of Engineer provides a very detailed classification based on three different level of screening, each of which corresponds to specific criterion that the soil has to fulfill in order to be classified as non-frost susceptible. These criteria are:

- Percentage of grains smaller than 0.02 mm
- Soil type according to the Unified Soil Classification System (USCS)
- Laboratory freezing test

Figure 1.5 depicts a graphical representation of this classification system, which divides soils into six categories according to their frost-susceptibility, ranging from negligible to very high:

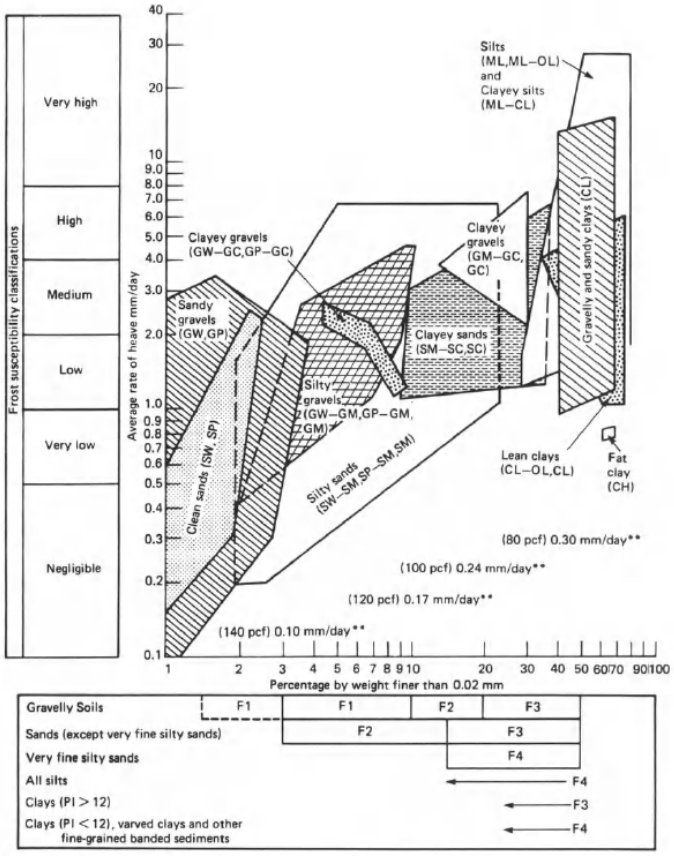

Figure 1.5: Frost susceptibility of soils (Department of the Army, 1965)

Little or no frost action is expected to occur in highly permeable soils such as sands, gravels and all other similar granular materials, where water is allowed to drain freely or freeze in-place without any segregation into ice lenses. On the contrary, silts and clayey silts are highly frost-susceptible soils due to their relatively good permeability and their high capillary rate. For what concerns clays, their impervious nature makes the frost heaving highly possible but not as severe as for silty soils, as water migration results to be slower (Christopher et al., 2006).

1.2.2 Thaw settlement

The downward movement of ground due to thawing processes is generally referred to as thaw settlement. The gradual melting of ice lenses into water leads to a new equilibrium void ratio to which the soil skeleton has to adapt, resulting in a volume change. This process, whose rate depends on both hydraulic properties of the soil, melting rate of the ice and applied loads, is known as thaw consolidation (Andersland and Ladanyi, 2004). It seems evident how ice content of frozen soil assumes an important role at this point. As a matter of fact, ice-rich soils are highly thaw sensitive and can produce significant settlement upon thawing, showing important loss in strength and bearing capacity (Ingeman-Nielsen, 2017). Thaw settlements are detrimental for buildings which can deform, as depicted in Figure 1.6.

Figure 1.6: Uneven permafrost thawing underneath a building foundation in Kangerlussuaq (Ingeman-Nielsen, 2017); vulnerability to subsidence is widespread in the Arctic due to seasonally natural freeze-thaw cycles but it is expected to increase under conditions of global warming (Nelson et al., 2001)

After the consolidation process is completed, the magnitude of thaw settlements is not necessarily as large as the displacement caused by frost heave. This was shown by Konrad (1989), who performed a series of freeze-thaw cycles tests on samples of clayey silt over a wide range of consolidation ratios. Results showed that the loading history prior to freezing and the number of freeze-thaw cycles to which the soil has been subjected to are important parameters. In particular, when a normal consolidated soil thaws after its first freeze-thaw cycle is likely to cause a settlement larger than the heave induced upon freezing (Konrad, 1989). This is especially important in those major underground projects in which artificial ground freezing is to be employed,

as the probability for soil to undergo its first freeze-thaw cycle is quite high and requires therefore more attention.
When the thawing process is slow, no excess pore pressure will develop as the released water can drain at the same rate as melting occurs. On the contrary, for faster thawing rates and in poorly permeable soils, a certain excess pore pressure may be generated due to undrained conditions. This implies a reduction in the effective stress level and a very low strength immediately after thawing (Harris, 1995). This significant strength reduction often leads to stability problems related to slopes or foundations, until the soil slowly regain its strength as it consolidates.

1.3 Artificial ground freezing

Despite frost action, it is often convenient to artificially freeze the soil in order to provide temporary stabilization and watertightness. Artificial ground freezing technique has been extensively used in the last decades as an effective and powerful construction method which provides ground support, groundwater control and structural underpinning during construction. However, the use of this technology requires a good knowledge of frozen soil behavior and a robust numerical model able to predict ground movements around the excavation. This is important especially in densely urbanized areas, where frost action is detrimental for surrounding structures. Artificial ground freezing is also a relevant technique in Arctic regions, as there is a growing need to keep soil frozen where permafrost thawing might be an issue due to global warming.

1.3.1 The technology

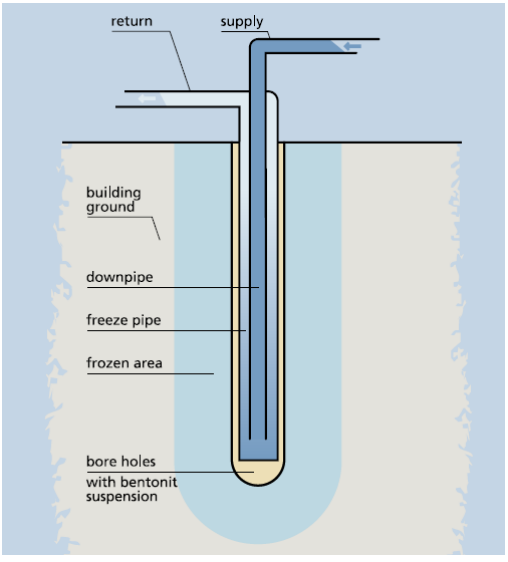

Figure 1.7: Basic principle of a freeze pipe and the refrigerant circuit (Max Bögl Group, 2018)

Artificial ground freezing (AFG) is a technique for temporarily increase soil strength and decrease its permeability. The technique consists of circulating coolant fluids, generally brine or liquid nitrogen, through buried pipes and thereby freezing of the pore water (Smith, 2012), as schematically illustrated in Figure 1.7. This process bonds soil particles together imparting great mechanical strength to the ground mass, which becomes highly watertight to seepage. These characteristics stabilize the ground and allow safe excavations nearby the frozen walls. The careful installation of suitably spaced pipes ensures eventually the overlapping of frozen soil columns and the formation of a strong and thick continuous wall within a certain time period (Smith, 2012). After the design temperature and thickness of the wall have been reached, a delicate maintenance stage takes place. During this phase, the heat extraction process is closely monitored to prevent any further advancement of the freezing front

and any deterioration due to uncontrolled thawing (Trevi S.p.a., 2013). Different stages relative to a tunnel construction are depicted in Figure 1.8:

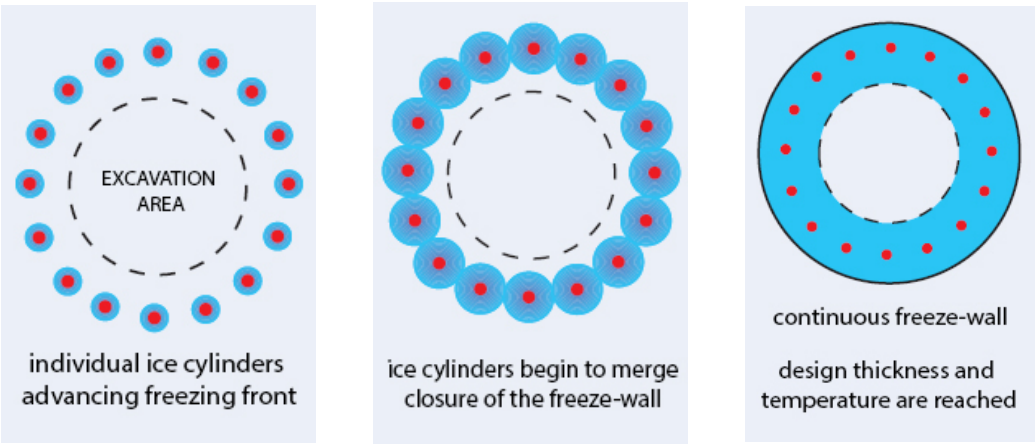

Figure 1.8: Schematization of the freezing stages adapted from Trevi S.p.a. (2013)

1.3.2 Freezing methods

The ground freezing can be carried out with four main different techniques:

- **brine freezing**, also known as indirect method or closed circuit, where a calcium chloride brine with freezing point between -40 °C and -50 °C is used.
- **liquid nitrogen freezing**, also known as direct method or open circuit with compressed gas in a liquid state at a temperature equal to -196 °C.
- **mixed method**, with liquid nitrogen used to initially quickly freeze the ground and then a brine system which accounts for the long-term freezing and/or in the maintenaince stage.
- **thermosyphons**, namely passive cooling systems consisting of a closed natural two phase convection device that extracts heat from the ground and discharge it into the environemnt.

The choice of application between the different methodologies is primarily due to economic considerations, jobsite locations and matters related to the timing required to the formation of the frozen soil volume (Rocca, 2011; Trevi S.p.a., 2013).

Brine freezing

Ground freezing with brine is the oldest available method, still implemented today. It is widely used in long-lasting interventions (more than 1 month) and when a significant volume of soil is involved (more than 500 m^3) (Rocca, 2011). In this technique, the brine is cooled to a temperature between -28°C and -35°C inside conventional refrigeration plants, normally using ammonia, and then pumped into the subterranean pipe system (Smith, 2012). The brine freezing method is outlined in Figure 1.9:

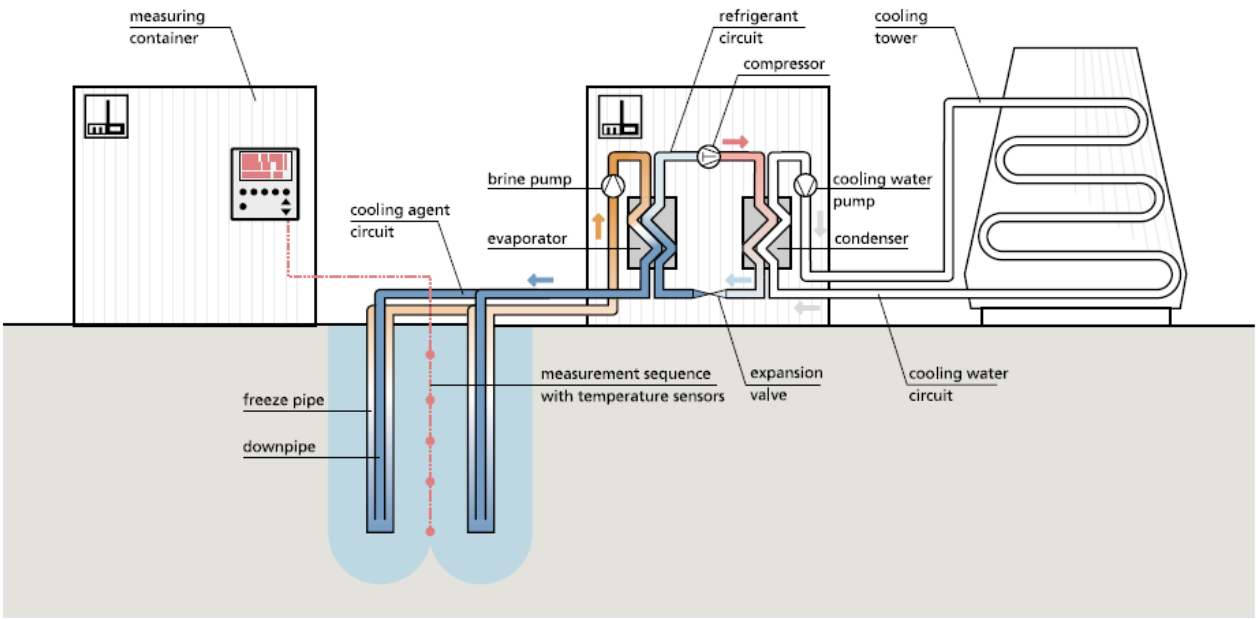

Figure 1.9: Conceptual model of the brine freezing technique (Max Bögl Group, 2018)

In the refrigeration system - or primary circuit - the ammonia is first brought to its liquid state by compressors and condensers, then gasified again in the evaporator by heat extraction from the brine solution which flows in the distribution system - or secondary circuit - with a pressure of 5 to 10 bars (Gallavresi, 1981; Rocca, 2011). The distribution system will typically consist of series-connected freezing pipes, thereby forming groups which are in turn connected in parallel. The freezing pipes are made up of two coaxial tubes: the brine flows downward into the inner tube and then circulates back through the existing cavity between the outer and inner tube (Rocca, 2011), guaranteeing a continuous heat withdrawal from the soil. The warmer brine solution is then fed back through return pipes to the refrigeration plant where it is re-chilled to start a new cycle, hence the name closed circuit. The implementation of the technology is characterized by a substantial capital investment due to the high cost of the refrigeration plant and a more complex coolant distribution system which requires skilled personnel around the clock. However, these expenditures are profitably compensated by the fact that the circuit is closed and therefore the volume of coolant fluid remains almost unchanged and the brine solution can either be disposed or recovered at the end of the intervention (Rocca, 2011). The process leading to the complete freezing of the soil, namely to that condition in which is safe to excavate, may take up to several months (Smith, 2012).

Liquid nitrogen freezing

In the case of short-term interventions characterized by reduced volume of soil involved (up to a few hundreds m^3 of ground), the liquid nitrogen freezing technique seems to be more appropriate (Rocca, 2011). Although the per-day cost is higher than with circulated brine, the method can be effectively employed in emergency situations, or in projects where the freeze has to be maintained for a short period of time.

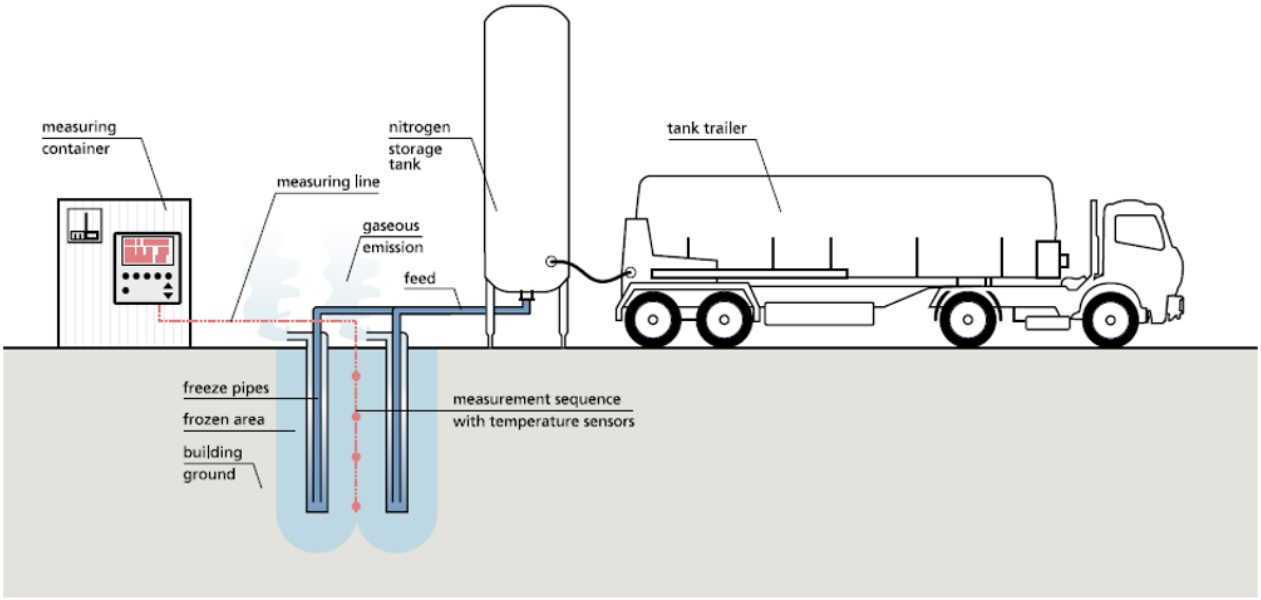

Figure 1.10: Conceptual model of the liquid nitrogen freezing technique (Max Bögl Group, 2018)

In this technique, special vacuum-insulated tankers are used to transport the liquid nitrogen at a temperature of -196 °C to the construction site. Here, they are temporarily stored waiting for the liquid nitrogen to be pumped into the freezing pipes and then vented to the atmosphere as a gas rather than re-circulated (Smith, 2012; Trevi S.p.a., 2013). A conceptual model of the system is depicted in Figure 1.10. The nitrogen freezing system is made up by one or more double-wall tanks with interposed vacuum, equipped with special evaporation-compression systems responsible for feeding the nitrogen into the freezing pipes with no need of pumps (Trevi S.p.a., 2013). As for the brine freezing, the liquid nitrogen circulates down a drop tube to the bottom of the freezing pipe and then flows back through the annular cavity, undergoing a phase change from liquid to gaseous and extracting heat from the soil. It is important that the nitrogen keeps its liquid state up to the entrance in the annular cavity inside the freezing pipes, where the larger section with respect to the inner tube will allow an expansion with the consequent phase change and the heat absorption equal to the nitrogen latent heat of vaporization (Rocca, 2011). The gas is then convoyed into the exhaust pipes and released into the atmosphere at a temperature between -60 °C and -120 °C. This is due to the fact that it is more convenient to purchase the new product rather than recover and re-compress the gaseous nitrogen, whose treatment plant may be difficult to place within the construction site. This translates in higher costs resulting from the continuous consumption of coolant fluid, which can nevertheless be largely offset by the shorter intervention time and lower cost of nitrogen storage and distribution facility (Smith, 2012; Rocca, 2011).

Thermosyphon technology

Artificial ground freezing can also be employed in Arctic regions where the aim is to thermally stabilize the warming permafrost underneath existing constructions and embankments. Since conventional freezing techniques require high operating costs and a significant amount of en-

ergy, their implementation is not always feasible in cold and remote locations. This is why passive cooling systems have been extensively used as alternative solutions in cold regions since 1960, thanks also to their good performance and low maintenance. Such systems consist of heat transfer devices, called thermosyphons, which rely on seasonally cold air to keep the ground frozen. A common thermosyphon is composed of a tube within which a coolant fluid is free to circulate. The tube can be divided into two sections: the first one buried in the ground - also known as condenser - and the second one exposed to the air - also known as evaporator. (Mu et al., 2016a). When the air temperature drops below that of the ground, the working liquid starts to evaporate rising towards the condenser where it is condensed and driven back to the evaporator section under gravity. In this way, the heat in the soil is transferred into the environment where it dissipates (Pan and Wu, 2002; Mu et al., 2016a). Such devices have been widely used in China along the Qinghai-Tibet Highway (QTH), the Qinghai- Tibet Railway and Qinghai-Tibet Power Transmission Line (QTPTL) where permafrost degradation of the plateau posed severe threats to the stability of these infrastructures (Mu et al., 2016a). Similar type of application can be found in Greenland, as shown in Figure 1.11, where however these devices are no longer maintained.

Figure 1.11: Thermosyphons installed in Kangerlussuaq to prevent permafrost from thawing beneath the buildings when the airport of the town was used as an American base during the Cold War. Photo taken in May 2017

1.3.3 Advantages and disadvantages

Rocca (2011) states that the technique is mostly used at present in loose or cohesive soils under the groundwater level, thus in presence of significant hydrostatic loads or especially when operating in urban environments. Nevertheless, soil heterogeneity and different freezing and thawing rates of materials should always be taken into account in the design phase, together with the groundwater flow conditions which may affect the freeze-wall formation and compromise a safe excavation (Andersland and Ladanyi, 2004).

When it comes to choose the more appropriate freezing technique for a specific project, it is necessary to make a few preliminary considerations regarding equipment, installation and costs, outlining advantages and disadvantages of the case to draw a selection criterion. The major difference between the methods lies in placing and operating the cryogenic treatment. While the open method only needs storage tanks for the liquid nitrogen, the brine freezing requires a complex and onerous capital investment concerning a refrigeration plant (Gallavresi, 1981). However, the initial cost is amortized during the operational phase, being the system closed and thus not requiring any additional expense in terms of new brine. On the contrary, liquid nitrogen is expensive and this normally reduces its application to short or very difficult interventions in need of remarkably high ground strength (Gallavresi, 1981). Therefore, combining the two techniques often seems to be the best solution when the difficulty of the project is high and involves soil heterogeneity, groundwater flows and considerable long freezing times (Trevi S.p.a., 2013; Gallavresi, 1981). Examples of the mixed method employement can be found in Naples and Rome Underground constructions (Viggiani and de Sanctis, 2009). An other important advantage of this technique lies in its eco-friendly nature, as no products are injected or dispersed in the soil. As a matter of fact, coolant fluids are never directly in contact with the soil or with the groundwater itself, thus avoiding any possible contamination of aquifers (Trevi S.p.a., 2013). To summarize benefits and drawbacks in terms of site installations and execution of freezing, Stoss and Valk (1979) developed a comparison between brine and liquid nitrogen methods, displayed in Table 2.1:

Table 1.1: Comparison between brine and liquid nitrogen freezing methods (Stoss and Valk, 1979)

Site installations	**Brine**	**Liquid nitrogen**
Pumps and electric power	required	not required
Water for cooling	required	not required
Refrigeration plant	required	not required
Storage tank	required	required
Pipe system for distribution coolant	supply and return	supply only
Low temperature material for surface pipes, valves, etc.	not required	required
Low temperature material for freeze pipes	not required	not required

Execution of freezing	**Brine**	**Liquid nitrogen**
Physical condition of coolant	liquid	liquid/vapour
Minimal temperature achievable (theoretic)	-55°C with $CaCl_2$	-196°C
Re-use of coolant	standard	impractical
Control of system	easy	difficult
Shape of frozen body	regular	often irregular
Temperature profile in frozen body	small differences	great differences
Frost penetration	slow	fast
Impact on frozen body in case of damage to freeze pipe	thawing effect	none
Noise	little	none

The success of freezing interventions can be verified on the basis of continuous monitoring and temperature data analysis in order to determine the state of ground freezing at a given time, this being defined in terms of achieved thickness of the frozen earth wall and thus in terms of its growth rate. In particular, the following aspects are monitored:

- **freeze pipe deviations**: as previously mentioned, soil freezing is realized by closely-spaced pipes distributed according to specific patterns depending on the type of project. Therefore, when this distance becomes important due to deviations of the boreholes and because of displacements associated with freeze-thaw cycles, poorly frozen areas or even frost gaps may occur and endanger the overall stability (Andersland and Ladanyi, 2004). To this purpose, best practice nowadays make use of borehole inclinometers which are able to trace the freeze pipe location.
- **temperature**: other monitoring systems include temperature sensors, which are used to control both the coolant fluid within the refrigeration system and the soil temperature around the excavation (Andersland and Ladanyi, 2004). Any abnormal data indicate areas of potential problems, therefore providing an early warning system to promptly react.
- **freezing front boundary location**: observations related to the frost advancement is based on the higher velocity of compression waves in ice (4000 m/s) with respect to water (1500 m/s). The seismic measurements are performed in situ by installing an energy source in one borehole and a geophone in a second one. In this way it is not only possible to locate the freezing front, but also to monitor the increase of thickness of the frozen earth wall by comparing travel times of compression waves (Andersland and Ladanyi, 2004).

1.3.4 Applications of freezing techniques

During the past 20 to 30 years ground freezing has been used as environmental remediation methods but more frequently for underground construction, tunneling, deep excavations, junctioning, underpinning of buildings and other special applications where control of groundwater flow was required (Haß and Schäfers, 2006). In many applications worldwide, ground freezing turned out to be the only reliable solution to create a watertight and load-carrying fully saturated soil body, where other conventional methods were not feasible. Van Dorst (2013) reports a list of the most significant European large-scale projects based on the fields in which they are applied and the construction year they were or will be finished:

Table 1.2: Large-scale European projects involving use of AGF adapted from Van Dorst (2013)

Tunnelling	**Junctioning**
Oslofjord subsea tunnel (2000)	The Netherlands Westerschelde Tunnel (2003)
Nuremberg-Fürth Underground Section 3.1.1 (2004)	Bremen Weser Tunnel (2003)
Munich Subway Station Marienplatz (2006)	Amsterdam Hubertus Tunnel (2008)
Amsterdam North/South Line: Damrak (2011)	Rotterdam Randstad Rail: Cross passages (2010)
Naples Subway Section Tratta Bassa (2015)	Antwerp Liefkenshoek Rail Link (2014)
Rome Subway Line C (under construction)	Cologne North South Urban Railway (2015)
Berlin Subway U5: Station Museumsinsel (2019)	Amsterdam North/South Line: Cross passages (2017)

Oslofjord subsea tunnel

The Oslofjord subsea tunnel is a 7.2 km long tunnel connecting Frogn and Hurum municipalities in southern Norway, running through a rock depression zone filled with glacifluvial materials (Eiksund et al., 2001). The weakness zone is located approximately 120 m below the sea level and it was first stabilized by grout injections and then by means of artificial ground freezing in order to proceed with the construction works in a controllable and safe manner. According to Eiksund et al. (2001), a total of 103 holes were drilled to allow the installation of freeze pipes in two rows from one side of the weakness zone, as illustrated in Figure 1.12. The freezing process was activated and maintained by brine, cooled by a refrigeration plant placed inside the tunnel for a period of approximately 12 weeks (Backer and Blindheim, 1999). The construction was successfully completed and the tunnel was open to the traffic in 2000.

Figure 1.12: Freeze pipes installed at Oslofjord tunnel for crossing the wakness zone (GEOFROST, 2018)

1.4 Research objectives

Freezing and thawing of pore water within soils involves a complex interaction between thermal, hydraulic and mechanical processes. Several models have been proposed in the last decades to tackle cold region geomorphological and geotechnical problems, with different degrees of complexity and sophistication (Nishimura et al., 2009). The primary aim of this MSc thesis is to evaluate the accuracy of the relatively new Elastic-Plastic Frozen/Unfrozen soil model, recently developed at the Norwegian University of Science and Technology (NTNU) by Ghoreishian Amiri et al. (2016b), in terms of predicting the temperature and displacement profiles of the ground subjected to artificial freezing in the construction of platform tunnels of Naples Underground. This translates in testing the model in real practical applications for the first time even though it has been previously validated against available element tests data and large-scale test data by Aukenthaler (2016) and Roostami (2017) and the necessary improvement has already been applied. Other aims of this MSc thesis are:

- Validate the reliability of the model for design and forecast approach in real and large-scale practical applications of artificial ground freezing, specifically the construction of the platform tunnel B1 at Garibaldi Station in Naples Underground
- Provide default values for the new constitutive model for rocks, especially for the yellow tuff (cemented, soft, volcanic rock) characterizing the subsoil of Naples and quite common in the Italian geological history

1.4.1 Research activities

The realisation of this MSc thesis was possible thanks to a series of research activities and thorough studies during the whole MSc program. The knowledge gained about infrastructure construction in cold regions during the DTU Arctic Semester in Greenland provides the basis on which it has been possible to build a more solid understanding of the topic in the remaining semesters. At NTNU, the following research procedure was followed:

- Literature review regarding the behaviour of frozen soil and freezing-thawing processes
- Literature review about artificial ground freezing technique and its consequences on soil and structures (partially carried out for the course "TBA4510 - Specialization Project")
- Getting familiar with the Elastic-Plastic Frozen/Unfrozen soil model in PLAXIS
- Learning fundamentals of Thermo-Hydro-Mechanical (THM) coupling and theoretical implementation of the Elastic-Plastic Frozen/Unfrozen soil model
- Understanding the meaning of the numerous model parameters
- Calibrating the model against known solutions in performed oedometer tests
- Validating the model in the practical application of the construction of Naples Underground with the necessary simplifying assumptions and applying modifications in case of discrepancies from available monitoring measurements

1.5 Methodology

By back-calculating available measurements of the tunneling project in the new underground of Naples, it has been possible to validate the new Elastic-Plastic Frozen/Unfrozen Soil model, as little data for artificial ground freezing in cold climate exists as of today but might be used in future. The numerical model is implemented in the Finite Element program PLAXIS 2D, which is used to evaluate the Thermo-Hydro-Mechanical response of the artificially frozen ground at Garibaldi station. Literature data, obtained by Pelaéz (2013) on Yellow Tuff retrieved from the subsoil of Naples were used to calibrate the constitutive model and propose default values for the model parameters. The model setup of platform tunnels was then possible afterwards, thanks to a collection of available data regarding construction phases, geometry and geology of the area.

1.5.1 Limitations

The objectives of this MSc thesis were partially hampered by the lack of available data regarding the implementation of the artificial ground freezing technique in the construction of Naples Underground. A series of simplifying assumptions were necessary in order to accommodate the scarcity of information and the final results may therefore have been affected.

1.6 Structure of the thesis

This MSc thesis consists of the following chapters:

- Chapter 1: **Introduction**
  This introductory chapter contains background information and a short overview of challenges related to frozen ground. In addition, the artificial ground freezing technique is presented to help the reader grasp its advantages and disadvantages. Motivation, research objectives related to the problem formulation, methodology and limitations are also included in this first chapter.
- Chapter 2: **A literature review**
  Here, frozen ground properties and behavior are illustrated by means of a comprehensive literature review. Major results have been collected from scientific papers and presented in this chapter.
- Chapter 3: **The constitutive model**
  This chapter contains a brief description of the Elastic-Plastic Frozen/Unfrozen Soil Model used as numerical tool in this MSc thesis. Its theoretical implementation, its last modifications and its ability to simulate frozen soil behavior are also discussed shortly.
- Chapter 4: **Calibration of the model**
  Here it is described the way in which the model was calibrated against available oedometer tests on samples retrieved from the subsoil of Naples. Through a back analysis and by trial and error it has been possible to feed the right input parameters into the model.
- Chapter 5: **Modeling of artificial ground freezing**
  This chapter includes a description of the project details of Naples Underground and specifically of Garibaldi Station. Here, the setup of the numerical model for the platform tunnel construction at Garibaldi Station is discussed and simulation results are presented.
- Chapter 6: **Conclusions**
  This is the final chapter of this MSc thesis and is comprised of final reflections and discussions about the obtained results. It also briefly summarizes the research contribution of this study, outlining recommendation for future works.

Chapter 2

Properties of frozen ground

2.1 Soil structure and phase relationship

Frozen soil constitutes a complex multi-phase system in which the voids are filled with ice, unfrozen water and air in different proportions. However, the soil might experience a fully frozen state at sufficiently low temperatures, where the system only consists of solid grains and pore ice. Figure 2.1 shows the dependency of unfrozen water content on temperature for three different soils. In particular, due to structure of the clay which is characterized by a significantly large specific surface, the unfrozen water content in this type of soil results to be the largest if compared with other materials. Conversely, in cohesionless soils with small specific surface like sand, this freezing point depression may be neglected. The presence of unfrozen water is due to that portion of water which is trapped within small crevices or bound to the surface of soil particles by means of chemical bonds and intermolecular forces (Spaans and Baker, 1996; Lackner et al., 2005). Even at temperatures well below the freezing point, this water will remain in the liquid phase for quite a long time, varying its amount according to temperature and type of soil, as depicted in Figure 2.1. In addition, Lackner et al. (2005) shows that freezing of these thin and liquid-like layers of water will eventually start where the level of binding is lowest, proceeding from the center of the pore towards its walls. Thus, the unfrozen water layer will progressively get thinner as temperature further drops, until most of the water is frozen at a temperature approximately equal to -70°C (Andersland and Ladanyi, 2004). According to Rempel et al. (2004) and Wettlaufer and Grae Worster (2006), two mechanisms (Figure 2.2) allow water to remain unfrozen even below its freezing temperature:

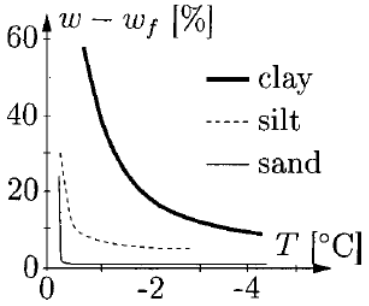

Figure 2.1: Unfrozen water content $w - w_f$ as function of the temperature T for different types of soil, where w and w_f are the water content of the unfrozen and frozen soil respectively (Andersland and Ladanyi, 2004)

1. **Curvature-induced premelting mechanism** which derives from the existence of water surface tension at the meniscus between soil particles, and acts by bonding grains together.

2. **Interfacial premelting mechanism** which results from repulsion forces arising between ice and soil grains. This mechanism acts by sucking in more water.

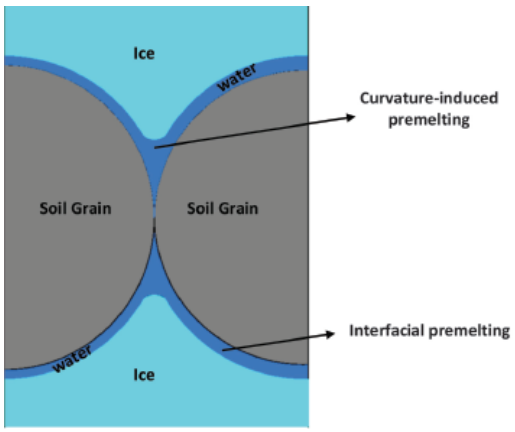

Figure 2.2: Schematic representation of the curvature induced premelting and interfacial premelting mechanisms (Ghoreishian Amiri et al., 2016b)

2.2 Mechanical properties

Frozen ground is also characterized by remarkably high strength, which depends upon soil frictional resistance, pore ice strength and the interaction between ice matrix and soil skeleton (Ting et al., 1983; Andersland and Ladanyi, 2004). The excellent bearing capacity that follows, allows heavy machinery to access the Arctic construction site during winter months, which otherwise would not be possible in the soft and muddy summer ground (Ingeman-Nielsen, 2017). Influence of ice content, temperature and confining pressure are also of importance when defining the strength of frozen soils and are therefore briefly discussed here:

- **ice content**: despite the presence of smaller amounts of unfrozen water, the mechanical behavior of frozen soils largely reflects that of the ice, whose strength is highly dependent on temperature. According to Sayles and Carbee (1981) and Andersland and Ladanyi (2004), the ice tends to dominate the mechanical response when the concentration of soil particles is less than 50 %. Other experimental results published by Baker (1979) and Ting et al. (1983) show that at lower ice content, strength of the soil mixture increases with increasing ice content, but after a certain threshold, the strength will decrease with increasing ice content. This can be explained by the existence of curvature-induced and interfacial premelting mechanisms, already briefly described. At lower ice content, the curvature-induced premelting mechanism dominates the frozen soil behavior resulting in higher strength. As the ice content increases, the interfacial premelting mechanism comes into play and determines strength weakening of the soil due to grains segregation and ice lens formation (Ghoreishian Amiri et al., 2016b).

- **temperature** represents the most influential parameter affecting frozen soil behavior, as it directly influences inter-granular ice strength, bonding robustness of grains-ice interface

and the unfrozen water content (Baker, 1979; Lai et al., 2010). Lower temperatures imply increased brittleness which at -10°C results to be more pronounced on frozen sand or silt than clay, whose behavior is kept plastic by the high enough unfrozen water content (Andersland and Ladanyi, 2004). It is worth to present here a series of uniaxial compression tests performed on a fine sand and a dense saturated clay at cryogenic temperatures. Bourbonnais and Ladanyi (1985b) show that tests on frozen sand present stress-strain curves with an increasingly brittle behavior with decreasing temperature, failing at axial strains of about 0.5 %, as shown left in Figure 2.3. Frozen over-consolidated clay with 25 % water content on the contrary, shows a plastic behavior despite decreasing temperature down to -110 °C and axial strains of over 5%; only at lower temperature, when eventually all the water is frozen, clay shows a brittle behavior as shown right in 2.3.

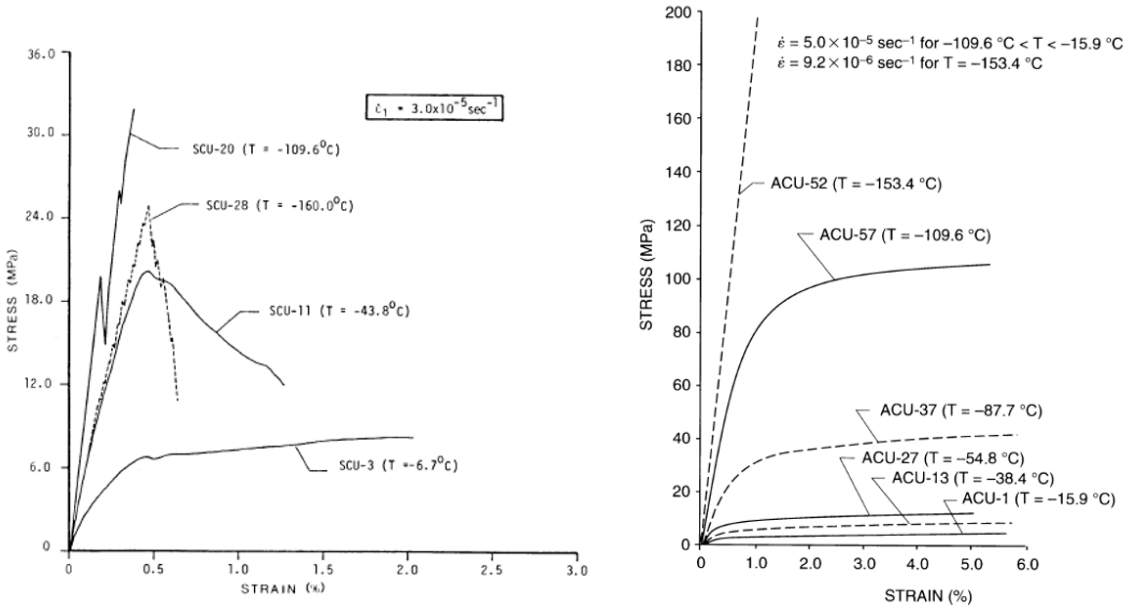

Figure 2.3: Low temperature stress-strain curve from uniaxial compression tests for frozen sand at left (Bourbonnais and Ladanyi, 1985b) and frozen clay at right (Bourbonnais and Ladanyi, 1985a)

- **confining pressure**: influence of this parameter on mechanical response of frozen soil has been reported by many researchers (Ladanyi, 1981; Arenson and Springman, 2005; Lai et al., 2010; Yuanming et al., 2010; Sinitsyn and Løset, 2011). Compression tests at constant strain rate and temperature, but a different confining pressures have been performed for example by Ladanyi (1981) on Ottawa sand and are illustrated schematically in Figure 2.4. Results show that at low confining pressures, the ice matrix is stiffer than the soil skeleton and reaches its first peak strength at small strain. The stress-strain curve is characterized by a brittle behavior in tension and strain softening in compression. This corresponds to the region A for pressure values up to 4 MPa. After a strain hardening stage in region B, the ice starts to take large portions of the normal pressure and begins to melt during shear.

Eventually, for pressure higher than 55 MPa, grains crush and pore ice thaws when entering region D. Since limited consolidation is allowed, shear failure occurs under undrained conditions assuming the same characteristic as in an unfrozen sand.

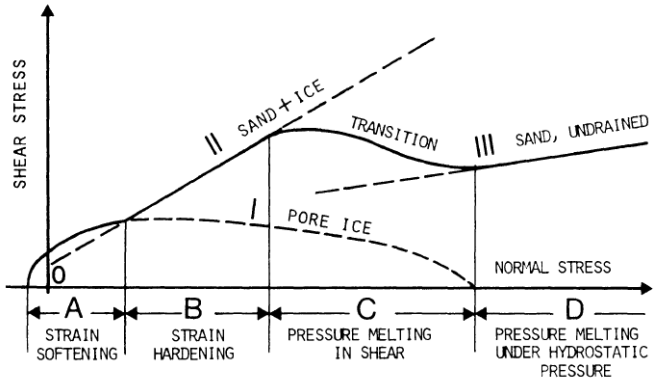

Figure 2.4: Complete failure envelope for frozen Ottawa sand in a normal stress vs. shear stress diagram. The envelope is the combination of three other failure lines which are: *line I* represents pore ice and includes regions A,B, and C between the tensile strength and the pressure melting point; *line II* depicts the the drained failure envelope of the sand-ice mixture resulting from internal friction and dilatancy; *line III* is the undrained failure line for unfrozen sand after melting of pore ice. (Andersland and Ladanyi, 2004)

2.3 Hydraulic properties

Flow in frozen soil is important in a number of periglacial processes such as patterned ground and soil creep (Burt and Williams, 1976). Furthermore, reduced hydraulic conductivity of frozen soil has also been exploited within environmental concerns. Benson and Othman (1996), Andersland et al. (1996) and Kirkelund and Jensen (2017) report that the frozen soil can be used as temporary waste-containment structure, since it behaves as an impermeable barrier to prevent further movement of contaminants and leakage from hazardous waste. As a matter of fact, some experiments conducted on different soil samples by Burt and Williams (1976) show that hydraulic conductivity decreases drastically with decreasing of temperature, as depicted in Figure 2.5. The impervious nature of frozen soil also allows engineers to control groundwater flow and proceed with safe excavations even below the water table (Harris, 1995).

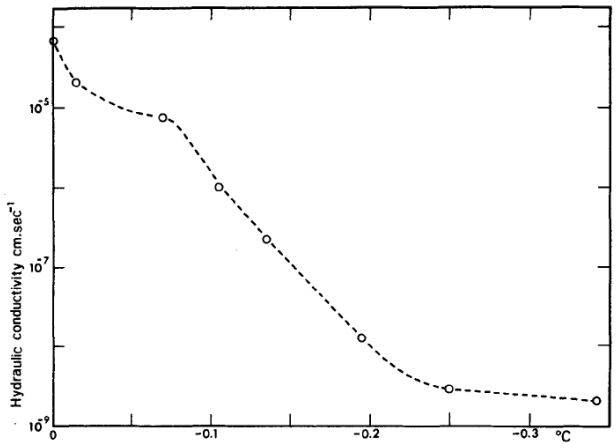

Figure 2.5: Dependence of hydraulic conductivity on temperature for a frozen clayey silt sample (Burt and Williams, 1976)

Chapter 3

The constitutive model

According to Ghoreishian Amiri et al. (2016b), the influence of ice content and temperature on the mechanical behavior of soil is the main difference between frozen and unfrozen state. Based on this statement, a new elastoplastic constitutive model (called Frozen and Unfrozen Soil Model) was developed at the Norwegian University of Science and Technology (NTNU) by Ghoreishian Amiri et al. (2016b) to describe the stress-strain behavior of saturated frozen ground. The model was later implemented as a user-defined soil model (UDSM) in PLAXIS. It is based on the Modified Cam Clay (MCC) model and it is formulated on the concept of two-stress state, that is solid-phase stress and cryogenic suction. This allows to build a complete thermo-hydro-mechanical (THM) framework where temperature, mechanical strength and hydraulic pressure are combined at the same time (Ghoreishian Amiri et al., 2016a). Their interaction is illustrated in the concept map by Thomas et al. (2009) in Figure 3.1:

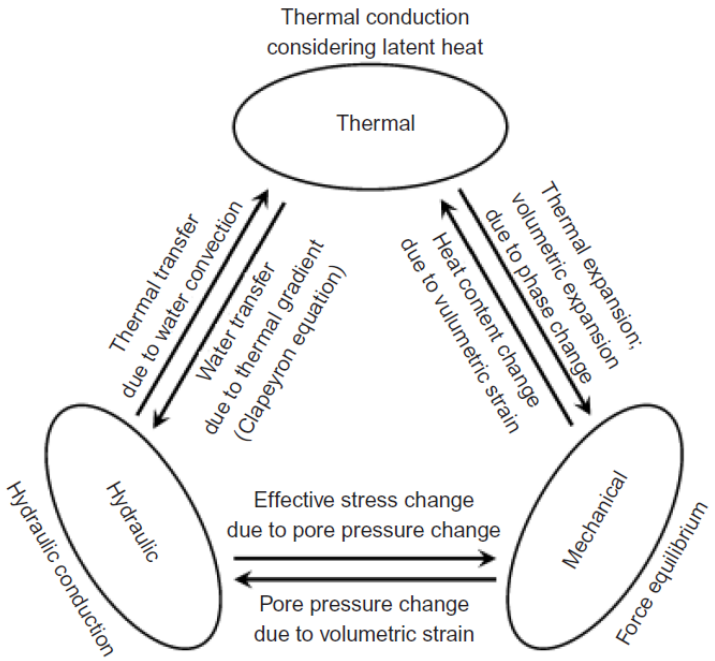

Figure 3.1: Thermo-hydro-mechanical interaction mechanism in frozen soil (Thomas et al., 2009)

3.1 Theoretical implementation

This section does not intend to be a detailed description of the theoretical implementation of the constitutive model for which one may refer to Ghoreishian Amiri et al. (2016a,b), but rather a brief discussion on its fundamental concepts. This will serve not only to get an overview of all the parameters involved, but also as an introduction to the last modification of the model. The overall description follows closely the one provided by Ghoreishian Amiri et al. (2016a,b).

3.1.1 Stress-state variables

The model is built on the assumption that both the soil skeleton and the ice are able to bear shear stresses. This allows to define the so-called solid phase stress σ^*, which can reflect the effects of unfrozen water in the soil. It is formulated as shown in Eq. 3.1:

$$\boldsymbol{\sigma}^* = \boldsymbol{\sigma} - S_{uw} p_w \boldsymbol{I} \tag{3.1}$$

where σ represents the sum of ice and soil grain stress, S_{uw} is the unfrozen water content, p_w is the water pressure and I is the unit tensor. The second stress state variable characterizing the model is cryogenic suction, which takes into account the effects due to ice content and temperature variation. This is defined as the difference between ice pressure p_i and water pressure p_w, and can be calculated using Clausius-Clapeyron equilibrium relation as in Eq. 3.2:

$$S_c = p_i - p_w \approx -\rho_i L \frac{T}{T_f} \tag{3.2}$$

where ρ_i is the ice density, L is the latent heat of fusion, T is the temperature of the system and T_f is the freezing/thawing temperature of water/ice at a given pressure. T_f is generally calculated by Eq. 3.3:

$$T_f = T_{f,ref} \left(\frac{p_i}{-p_{0,ref}} + 1 \right)^{\frac{1}{\alpha}} \tag{3.3}$$

where $T_{f,ref}$ is the reference temperature of 273.16 K, $p_{0,ref}$ is the corresponding reference pressure equal to -395 MPa and α is a constant commonly selected between 7 and 9.

3.1.2 Strain decomposition

Like any other soil model, the decomposition of strain increment $d\varepsilon$ has to be defined. This is given by Eq. 3.4:

$$d\varepsilon = d\varepsilon^{me} + d\varepsilon^{se} + d\varepsilon^{mp} + d\varepsilon^{sp} \tag{3.4}$$

where $d\varepsilon^{me}$ and $d\varepsilon^{mp}$ are respectively the elastic and plastic strain increments due to solid phase stress variation, while $d\varepsilon^{se}$ and $d\varepsilon^{sp}$ refer respectively to the elastic and plastic strain increments this time due to a variation of the cryogenic suction.

3.1.3 Yield surfaces

When the value of cryogenic suction becomes zero, the soil is in its unfrozen state and the model reduces to a conventional Modified Cam Clay model. When the soil is frozen on the other hand, to account for the premelting effects already described in Section 2.1, it is necessary to define two suction-dependent yield surfaces, that is Loading Collapse (LC) and Grain Segregation (GS) yield surfaces. The former, by expanding with increasing cryogenic suction, takes into account the curvature-induced premelting mechanism that bounds soil grains together. The latter comes into play when the premelting dynamic behavior is dominated by interfacial premelting mechanism which is responsible for a soil expansion due to grain segregation and ice lens formation. While the curvature-induced premelting mechanism results in a compressive deformation and it is considered to constitute the elastic part of the deformation due to suction variation, the interfacial premelting mechanism accounts for those irrecoverable strains and thus the plastic part of the deformation. LC and GS yield surfaces may be mathematically defined by Eq. 3.5 and Eq. 3.6 respectively, but more details about their formulation can be found in Ghoreishian Amiri et al. (2016a,b) and Aukenthaler (2016).

$$F_1 = (p^* - k_t s_c)[(p^* - k_t s_c) S_{uw}^m - (p_y^* - k_t s_c)] + \frac{(q^*)^2}{M^2} = 0 \tag{3.5}$$

$$F_2 = s_c - sc, seg = 0 \tag{3.6}$$

where p^* is the solid phase mean stress, k_t describes the increase in apparent cohesion with cryogenic suction s_c, S_{uw} is the unfrozen water content, m is a yield parameter, q^* is the solid phase deviatoric stress, M is critical state line (CSL) slope, p_y^* is the preconsolidation pressure for frozen conditions and $s_{c,seg}$ is the threshold value of suction for the ice segregation phenomenon. Figure 3.2 shows a 3D view of the yield surfaces:

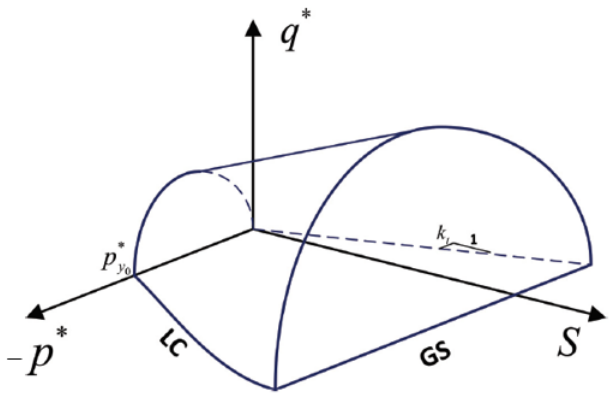

Figure 3.2: Three-dimensional view of Loading Collapse (LC) and Grain Segregation (GS) yield surfaces. The line with slope k_t is called Ice Tension Line (ITL) and it represents the soil ability to bear tensile stresses with cryogenic suction (Ghoreishian Amiri et al., 2016a)

3.1.4 Coupled hardening rules

The position of yield surfaces in the space is controlled by irreversible deformations taking place. According to Ghoreishian Amiri et al. (2016a), a plastic compression due to a variation in the solid phase stress will result in a stiffer behavior of the soil and a reduction in the dimension of voids, namely implying a lower segregation threshold valued. In terms of yield surfaces, this translates into the LC surface moving outward, whilst the GS shifts downward. On the contrary, a plastic dilation caused by the occurrence of ice segregation will force the GS to move upward and the LC to move inward, resulting in a softer behavior of the soil. The hardening rules for the LC and GS yield surfaces are given by Eq. 3.7 and Eq. 3.8 respectively:

$$\frac{dp^*_{y0}}{p^*_{y0}} = -\frac{1+e}{\lambda_0 - \kappa_0}(d\varepsilon_v^{mp} + d\varepsilon_v^{sp}) \tag{3.7}$$

$$\frac{ds_{c,seg}}{s_{c,seg} + p_{atm}} = \frac{1+e}{(\lambda_s + \kappa_s)} d\varepsilon_v^{sp} + \frac{1+e}{\lambda_s + \kappa_s}\left(1 - \frac{s_c}{s_{c,seg}}\right) d\varepsilon_v^{mp} \tag{3.8}$$

where p^*_{y0} denotes the preconsolidation pressure for unfrozen conditions, e is the void ratio, $d\varepsilon_v^{sp}$ is the cryogenic suction volumetric plastic strain and $d\varepsilon_v^{mp}$ is the mechanical volumetric plastic strain such as in the MCC model. When it comes to λ and κ, these are the elastoplastic and elastic compressibility coefficients respectively, and their subscripts indicate whether they are referred to the unfrozen state (0) or to a suction variation (s). Figure 3.3 and Figure 3.4 depict respectively the evolution of yield surfaces due to plastic compression and dilation:

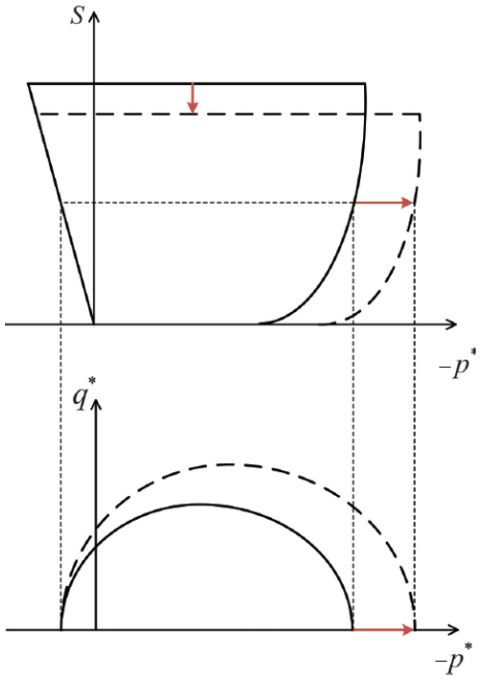

Figure 3.3: Evolution of yield surfaces due to plastic compression (Ghoreishian Amiri et al., 2016a)

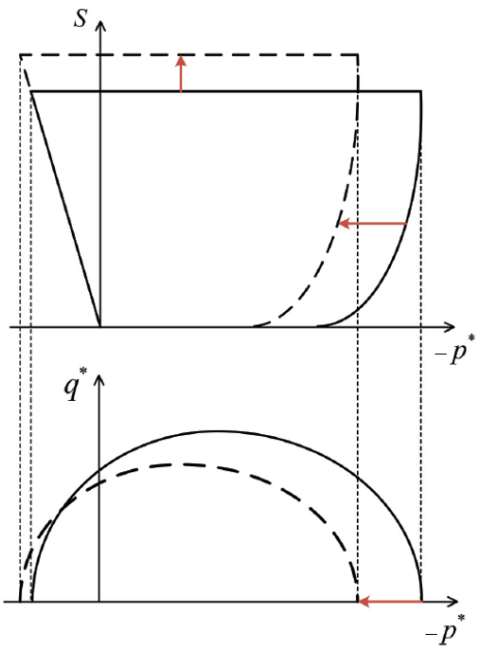

Figure 3.4: Evolution of yield surfaces due to plastic dilation (Ghoreishian Amiri et al., 2016a)

The hardening rule for the GS yield surface also takes into account that the amount of strain due to interfacial premelting mechanism depends on the availability of water. In a low water saturated soil, even though temperature decreases and cryogenic suction increases, there is no possibility for the volume to dilate. In light of this statement, the GS yield surface should be able to shift upward without any change in volume. This is also consistent with the reality as frost heave will not develop if water is not provided (Aukenthaler, 2016).

3.1.5 Destructuration

Newly, a modification has been incorporated in the model to take into account the structure loss of the soil due to freeze-thaw cycles. This improvement allows the model to achieve a better representation of ground behavior and its complex aspects. The destructuration phenomenon begins when pore water starts to freeze, resulting in a structural change within the soil. Ice formation and thawing will produce a degradation of the bonds between particles or aggregates that compose the soil. Mathematically, the structure loss translates into the addition of a new parameter c_{str} in the expression given by Eq. 3.9:

$$\frac{dp^*_{y0}}{d\max s_i} = c_{str}\frac{r}{\lambda} \tag{3.9}$$

where

$$\lambda = \lambda_0[(1-r)\exp(-\beta s_c) + r] \tag{3.10}$$

where $\max s_i$ denotes the maximum ice saturation that the ground has experienced so far, r is related to the maximum stiffness of the soil for an infinite value of cryogenic suction, λ refers to the partially frozen state elastoplastic compressibility coefficient and β is a parameter controlling the rate of change in soil stiffness with cryogenic suction.

3.1.6 Flow rules

A non-associated flow rule, which makes use of a different surface as plastic potential, is used for the LC yield surface. The flow rule and the plastic potential function Q_1 are given respectively by Eqs. 3.11 and 3.12:

$$d\varepsilon^{mp} = d\lambda_1\frac{\partial Q_1}{\partial \boldsymbol{\sigma}^*} \tag{3.11}$$

$$Q_1 = S_{uw}^{\gamma}\left(p^* - \frac{p^*_y + k_t s_c}{2}\right)^2 + \left(\frac{q^*}{M}\right)^2 \tag{3.12}$$

in which the exponent γ is the plastic potential parameter controlling the volumetric behavior. Aukenthaler (2016) states that by increasing ice content, the plastic potential surface will become a straight line as the tendency of volume change decreases by increasing ice saturation. Regarding the GS yield surface, an associated flow rule is used instead as given by Eq. 3.13:

$$d\varepsilon^{sp} = -d\lambda_2 \frac{\partial F_2}{\partial s_c} \boldsymbol{I} \tag{3.13}$$

Notice that $d\lambda_1$ and d $d\lambda_2$ are plastic multipliers for the LC and GS yield surfaces respectively. They may be obtained by imposing plastic consistency conditions (Aukenthaler, 2016).

3.2 Model parameters

The current version of the model requires 26 input parameters, listed in Table 3.1, in addition to soil properties and certain known thermal parameters of water and ice which will be described and introduced in the next chapter.

Table 3.1: Input parameters to the Frozen and Unfrozen Soil Model (Ghoreishian Amiri et al., 2016a)

Parameter	**Description**	**Unit**
T_{ref}	Reference temperature	K
$E_{f,ref}$	Frozen soil Young's modulus at reference temperature	N/m^2
$E_{f,inc}$	Rate of change in Young's modulus with temperature	$N/m^2/K$
ν_f	Frozen soil Poisson's ratio	-
G_0	Unfrozen soil shear modulus	N/m^2
κ_0	Unfrozen soil elastic compressibility coefficient	-
p_c^*	Reference stress	N/m^2
λ_0	Unfrozen elastoplastic compressibility coefficient	-
γ	Plastic potential parameter	-
k_t	Rate of change in apparent cohesion with suction	-
M	Slope of the critical state line (CSL)	-
λ_s	Elastoplastic compressibility coefficient for suction variation	-
κ_s	Elastic compressibility coefficient for suction variation	-
r	Coefficient related to the maximum soil stiffness	-
β	Rate of change in soil stiffness with suction	$(N/m^2)^{-1}$
m	Yield parameter	-
$(p_{y0}^*)_{in}$	Initial preconsolidation stress for unfrozen conditions	N/m^2
λ_r	Fitting parameter for unfrozen water saturation curve	-
ρ_r	Fitting parameter for unfrozen water saturation curve	N/m^2
Y_{ref}	Reference coordinate for $(p_{y0}^*)_{in}$ with depth	m
Δp_{y0}^*	Rate of change in p_{y0}^* with depth	$N/m^2/m$
e_0	Initial void ratio	-
$(S_{c,seg})_{in}$	Initial segregation threshold	N/m^2
α	Parameter for the pressure dependency of ice thawing temperature	-
$p_{0,ref}$	Reference pressure for ice thawing	N/m^2
K_w	Water bulk modulus	N/m^2
c_{str}	Structural parameter	N/m^2

Chapter 4

Calibration of the model

A correct and reliable simulation outcome is certainly due to the right choice of input parameters, whose determination is generally related to laboratory testing. In this particular case, an oedometer test was run on Neapolitan yellow tuff under freezing and thawing conditions by Pelaéz (2013). The test has been reproduced in PLAXIS and treated as a boundary value problem (BVP) in order to obtain a best-fit of the simulated results with the test results. This guarantees the correctness of chosen input parameters, which thus are representative of the THM behavior of the ground in Naples. Due to the lack of other available laboratory tests, it has been necessary to guess the majority of input parameters within a reasonable range, proceeding by trial and error. This process has been laborious and time-consuming due to the amount of required input parameters in the model.

4.1 Oedometer test model setup

The experimental set-up used by Pelaéz (2013) was composed of an oedometer cell immersed in a thermal bath and equipped with thermocouples for temperature monitoring in the sample.

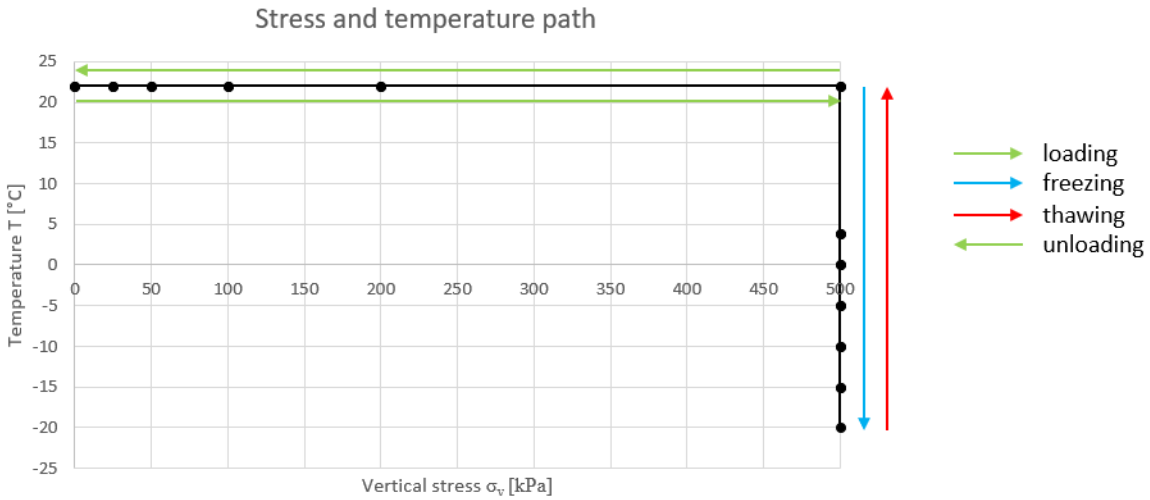

Figure 4.1: Stress and temperature paths followed during the oedometer test performed on a sample of yellow tuff (Pelaéz, 2013)

The test has been performed by applying an incremental step loading each 24 hours at the top of the sample (25 → 50 → 100 → 200 → 500 kPa) and at a constant temperature of 22°C. Then, a freeze-thaw cycle (+22 ↔ 4 ↔ 0 ↔ -5 ↔ -10 ↔ -15 ↔ -20°C) was applied by step every 6 hours at constant vertical stress of 500 kPa, that was considered the representative in-situ vertical stress. Eventually, an unloading phase by 24 hours step (500 → 200 → 100 → 50 → 25 kPa) took place at constant temperature of 22°C. The overall stress path is depicted in Figure 4.1. As already mentioned previously, this oedometer test has been reproduced in PLAXIS as a plane strain BVP with 6-noded elements medium mesh. The scaled model geometry is shown in Figure 4.2:

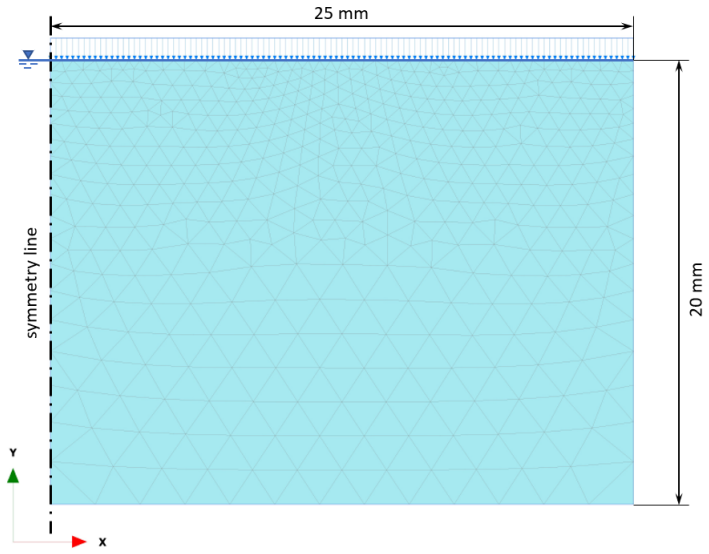

Figure 4.2: Model geometry in PLAXIS, where only half of the sample has been modelled due to symmetry reasons

4.1.1 Boundary conditions

The sample is fully saturated and all the boundaries, except the bottom one, are closed for water flow and hence no seepage is allowed through them. The drainage type has been however set to *drained* as water flow is allowed through the bottom of the sample. For what concerns thermal boundary conditions, these have been applied to all boundaries, except the left vertical one which corresponds to a symmetry line. In particular, time-dependent temperature functions have been assigned to the boundaries according to the thermal loading provided during the experimental test.

4.1.2 Set of soil parameters

The boundary value problem requires the provision of general soil properties which every other soil model would require as well. Most of the basic properties of the yellow tuff were found in literature and have been used as input parameters (Colombo et al., 2009; L'Amante et al., 2012; Pelaéz, 2013; Papakonstantinou et al., 2010, 2013; Mandolini and Viggiani, 2017; Fabozzi et al., 2017). Exception is made for the thermal expansion $\alpha_{x,y,z}$ which has been back-calculated by best-fit of test results. It should noticed moreover that the thermal conductivity of the rock is

significantly low, if compared to other materials. Soil properties used for this model calibration are listed in Table 4.1:

Table 4.1: Input parameters related to soil general properties divided into PLAXIS tab sheets

	Parameter	Description	Value
General tab sheet	γ_{sat}	Saturated unit weight [N/m^3]	$16 \cdot 10^3$
	γ_{unsat}	Unsaturated unit weight [N/m^3]	$16 \cdot 10^3$
	e_0	Initial void ratio [-]	1,38
Groundwater tab sheet	k_x	Hydraulic conductivity in x-direction [m/s]	$0,01 \cdot 10^{-3}$
	k_y	Hydraulic conductivity in y-direction [m/s]	$0,01 \cdot 10^{-3}$
Thermal tab sheet	c_s	Specific heat capacity [J/(Kg · K)]	700
	ρ_s	Density of the solid material [Kg/m^3]	2718
	λ_{s^1}	Thermal conductivity [W/(m · K)]	0,492
	$\alpha_{x,y,z}$	Thermal expansion coefficient in x, y, z directions [1/K]	$5 \cdot 10^{-6}$
Initial tab sheet	$K_{0x,0y}$	At rest earth pressure coefficient [-]	0,9825

4.1.3 Thermal parameters of water and ice

Another group of input parameters are related to the thermal properties of water and ice. These are standard tabulated values which can be found by default in PLAXIS or in literature. They are listed in Table 4.2:

Table 4.2: Input parameters related to thermal properties of water and ice

	Parameter	Description	Value
Water	γ_{water}	Unit weight [N/m ^{3}]	$10 \cdot 10^3$
	c_{water}	Specific heat [J/Kg · K]	4190
	$\lambda_{s^1,water}$	Thermal conductivity [W/m · K]	0,6
	L_{water}	Specific latent heat [J/Kg]	$344 \cdot 10^3$
	α_{water}	Thermal expansion coefficient [1/K]	$0,21 \cdot 10^{-3}$
	T_{water}	Temperature [K]	277,16
Ice	c_{ice}	Specific heat [J/Kg · K]	2095
	$\lambda_{s^1,ice}$	Thermal conductivity [W/m · K]	2,2
	α_{ice}	Thermal expansion coefficient [1/K]	$0,05 \cdot 10^{-3}$

4.1.4 Hydraulic model

According to Nishimura et al. (2009), the THM modeling requires a freezing characteristic function to relate the unfrozen water content S_{uw} to the thermodynamic properties of the soil. In particular, the van Genuchten hydraulic model was employed to describe the freezing characteristic function in PLAXIS, which is given by Eq. 4.1:

$$S_{uw} = \left[1 + \left(\frac{s_c}{\rho_r} \right)^{\frac{1}{1-\lambda_r}} \right]^{-\lambda_r} \tag{4.1}$$

In order to assess the values of input parameters λ_r and ρ_r, Eq.4.1 was fitted with the power law of Tice et al. (1976), which is given by Eq. 4.2 and returns experimental values for the unfrozen water content:

$$S_{wu} = \alpha \cdot \left| \frac{T}{T_{ref}} \right|^{-\beta} \qquad (T < T_0) \tag{4.2}$$

where α and β are material constants findable in literature and T_{ref} is a reference temperature of 1°C introduced for dimensional reasons. It should be mentioned that there is no available documentation regarding thermal properties of the ground in Naples. The values of $\alpha = 0,8$ and $\beta = 0,727$ were therefore selected for a generic type of rock due to the lack of data related to the Neapolitan yellow tuff. Neverthless, a good match was achieved, as shown by Figure 4.3. The values of λ_r and ρ_r turned out to be 0,41 [-] and $800 \cdot 10^3$ [N/m ^{2}] respectively.

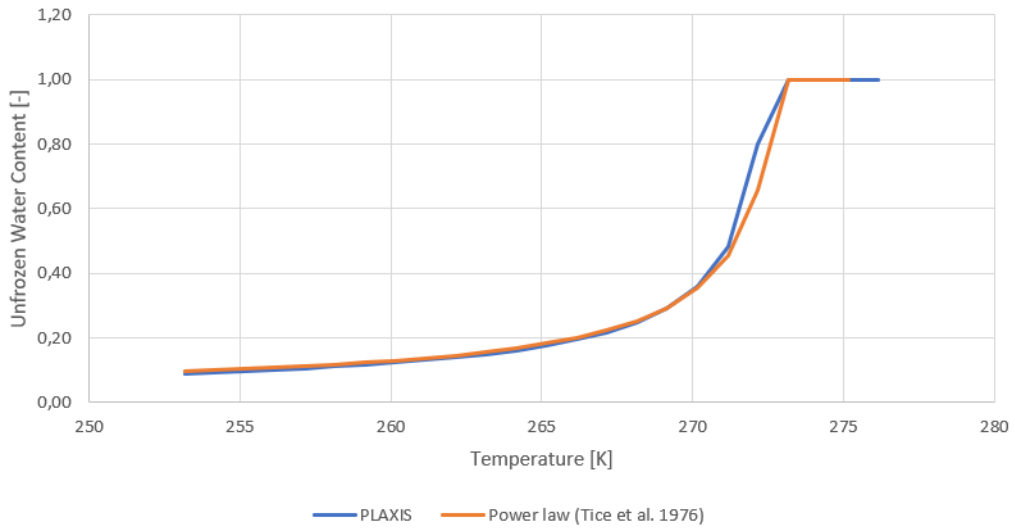

Figure 4.3: Curve fitting between the power law and the freezing characteristic function. The plateau after 273,16 K indicates that all the water is in the unfrozen state.

Other input parameters related to the hydraulic component of the constitutive model are associated with the original formulation of the van Genuchten model (Brinkgreve et al., 2016), according to which water saturation can be expressed as function of pressure head ϕ_p as shown in Eq. 4.3:

$$S(\phi_p) = S_{res} + (S_{sat} - S_{res}) \left[1 + \left(g_a \left|\phi_p\right|\right)^{g_n}\right]^{g_c} \tag{4.3}$$

where:

- ϕ_p is defined as the negative ratio between the suction pore stress p_w and the unit weight of water γ_w.
- S_{res} denotes a residual saturation, that is when a part of the fluid remains in the pores even at high suction heads. It should attain a value close to 0.

- S_{sat} represents the saturation degree. It comes into play when pores are filled with both water and air. It is assumed by default equal to 1 under fully saturated conditions.
- g_n, g_a and g_c are fitting parameters which can be easily calculated as follows:

$$g_a = \frac{\gamma_w}{\rho_r}, \qquad g_c = -\lambda_r, \qquad g_n = \frac{1}{1-\lambda_r} \tag{4.4}$$

Table 4.3 summarizes the input parameters associated with the hydraulic model, specifying the relative adopted values in this calibration. For simplicity, they are again divided according PLAXIS tab sheets.

Table 4.3: Input parameters associated with the hydraulic model

	Parameter	**Description**	**Value**
Groundwater tab sheet	S_{res}	Residual saturation [-]	0,02
	S_{sat}	Degree of saturation [-]	1
	g_n	Fitting parameter 1 [-]	1,590
	g_c	Fitting parameter 2 [-]	-0,41
	g_a	Fitting parameter 3 [1/m]	0,04
Parameter tab sheet	ρ_r	Fitting parameter 4 [N/m ^{2}]	$800 \cdot 10^3$
	λ_r	Fitting parameter 5 [-]	0,41

4.1.5 Constitutive model parameters

Finally, the rest of input parameters have been selected by guessing their most likely range and then proceeding by trial and error. Their values are listed in Table 4.4. This process has been demanding and time-consuming both because of the large number of parameters involved but also because a very limited amount of literature is present concerning frozen behavior of pyroclastic materials, like Neapolitan yellow tuff.

Table 4.4: Input parameters to the constitutive model for the BVP

Parameter	**Value**	**Value**	**Value**
T_{ref} [K]	273,16	κ_s	$0,5 \cdot 10^{-3}$
$E_{f,ref}$ [N/m^2]	$50 \cdot 10^6$	r [-]	0,04
$E_{f,inc}$ [N/m^2/K]	$10 \cdot 10^6$	β [(N/m^2)$^{-1}$]	$0,8 \cdot 10^{-6}$
ν_f [-]	0,45	α [-]	9
G_0 [N/m^2]	$700 \cdot 10^6$	$p_{0,ref}$ [N/m^2]	$-395 \cdot 10^6$
κ_0 [-]	0,01	m [-]	1
p_c^* [N/m^2]	$-40 \cdot 10^3$	$(p_{y0}^*)_{in}$ [N/m^2]	$-500 \cdot 10^3$
λ_0 [-]	0,05	Y_{ref} [m]	0
γ [-]	1	Δp_{y0}^* [N/m^2/m]	0
k_t [-]	0,09	$(S_{c,seg})_{in}$ [N/m^2]	$20 \cdot 10^6$
M [-]	1,11	K_w [N/m^2]	10^9
λ_s [-]	0,85	c_{str} [N/m^2]	$-200 \cdot 10^3$

4.2 Results

The model was successfully calibrated against the oedometer test data collected by Pelaéz (2013). Accumulated deformations were plotted in a void ratio vs. applied vertical stress diagram and superposed to the experimental results. As shown in Figure 4.4, the match is fairly good, despite the presence of a slight shift between the curves.

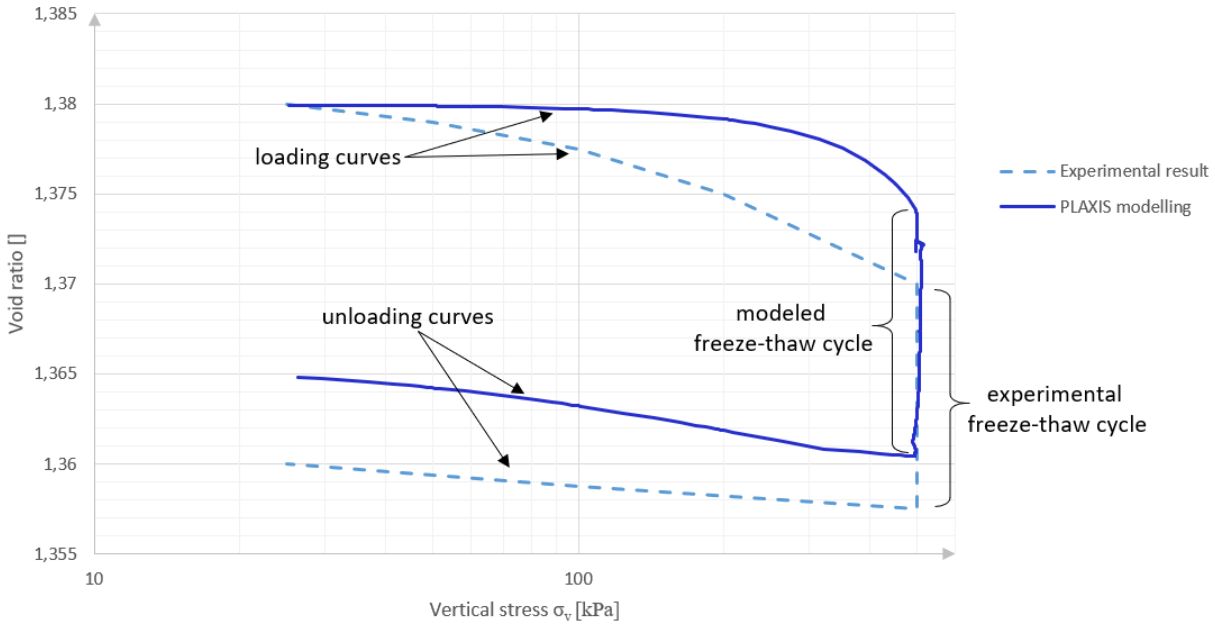

Figure 4.4: Fitting of the experimental curve with the simulated results from PLAXIS

Loading and unloading were controlled mainly by the unfrozen elastic and elastoplastic compressibility coefficients, that is κ_0 and λ_0 respectively. These parameters represent the slope of the loading curve before and after the unfrozen pre-consolidation stress, which also plays an important role in the modeling. As it can be observed by Table 4.4 low values of κ_0 and λ_0 were selected to take into account the stiffer behavior of the tuff compared to any other type of soil. Although lower values could have been chosen to reduce the gap between modeled and experimental curves, this would have caused an undesired plastic behavior during unloading. During the freeze-thaw cycle, there is a change in void ratio equal to $\Delta e_0 = 0,014$ against lab results giving a variation of $\Delta e_0 = 0,012$. The reason for this structural loss occurring nearly entirely during thawing is to be found in the physical degradation of the bonds between the grains. When water freezes and expands, it is responsible for breaking these structural bonds. Newly formed ice is however capable at the same time to provide structural support by bonding soil particles together. Issues arise when melting ice is not longer able to provide that structural support to the ground, which therefore undergoes an irreversible reduction of the void ratio and loss in structure. Apart from c_{str} which controls the destructuration phenomenon, the freeze-thaw cycle is also affected by the initial segregation threshold $(S_{seg})_{in}$ for which an extremely high value was selected. This is due to the fact that no heave was observed during lab testing and therefore no heave was desired during modeling. The segregation threshold can be iden-

tified in a cryogenic suction vs. specific volume diagram, as shown in Figure 4.5. Here it can be noticed that the increase in cryogenic suction s_c will cause a decrease of the specific volume with a rate controlled by the elastic compressibility coefficient for frozen conditions κ_s. On the contrary, specific volume will increase after the segregation threshold with a rate controlled by the elastoplastic compressibility coefficient for frozen conditions λ_s. Hence, for extremely large and unreachable values of the segregation threshold, λ_s is actually off and does not affect the calculation, as in this case.

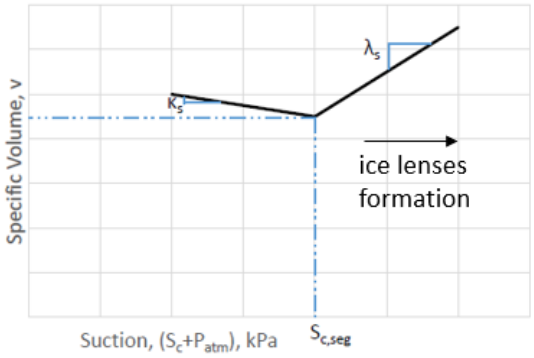

Figure 4.5: General behavior of soil sample under isotropic thermal loading (adapted from Roostami (2017))

4.2.1 Other outputs

It is worth mentioning here that PLAXIS also allows to inspect other types of outputs. Even though these cannot be compared with experimental results due to lack of available data, they provide useful information about freezing front advancement, hence temperature distribution and ice saturation within the sample. An example is shown in Figures 4.6 and 4.7.

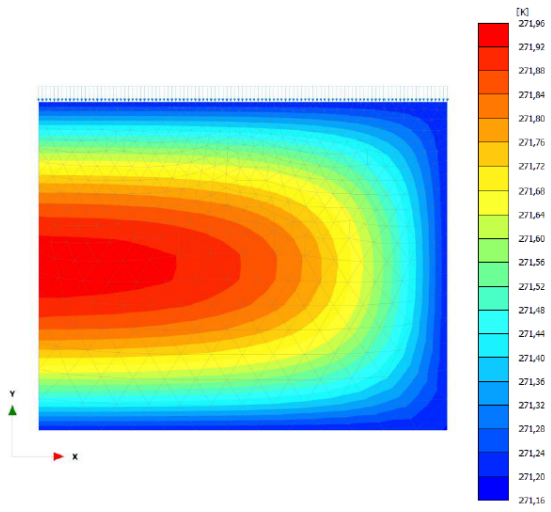

Figure 4.6: Example of temperature distribution within the sample when freezing to -2°C. The left boundary is a symmetry line.

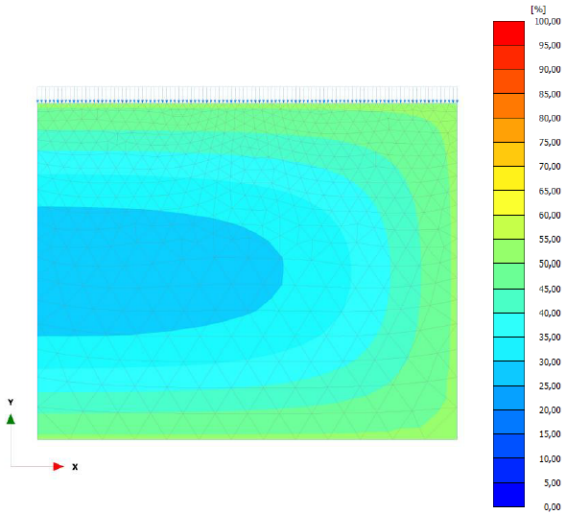

Figure 4.7: Example of ice saturation within the sample when freezing to -2°C. The left boundary is a symmetry line.

Chapter 5

Modeling of artificial ground freezing

After the model has been calibrated and the behavior of the Neapolitan yellow tuff upon freezing and thawing correctly predicted, it is possible to simulate the railway tunnel construction in Naples. After a brief illustration of the Line 1 project, this chapter deals with the description of platform tunnel construction at Garibaldi Station and the implementation of its corresponding model in PLAXIS. Final results of the THM simulation are outlined at the end of this chapter and compared with the settlement history at the reference point B8 (see Figure 5.5) in the proximity of Garibaldi Station.

5.1 Naples underground metro

The final design of the Line 1 of Naples underground metro consists of a 40 km (25 stations) closed ring snaking its way through the northern part of the city, the airport, the administrative district, the historical center and the area of the hills (Viggiani and de Sanctis, 2009), as depicted in Figure 5.1.

Figure 5.1: Route of Line 1 of Naples underground metro (Viggiani and Casini, 2015)

The construction of the so-called Tratta Bassa, namely the section between the stations of Dante and Garibaldi, has been accomplished by means of artificial ground freezing. This technique resulted to be particularly suitable for tunneling in a such densely urbanized areas like the historic city center of Naples, where preserving the integrity of the overlying buildings was one of the most important construction requirements. The size of the man-made freezing intervention was significant: for each station, a volume of approximately 33.000 m^3 of ground was frozen to permit the excavation of the four section tunnels and the corresponding four inclined passageways (Colombo, 2010).

5.1.1 Ground conditions

Ground conditions in Naples are described by many researchers (Viggiani and de Sanctis, 2009; Russo et al., 2012; Papakonstantinou et al., 2013, 2010; Pelaéz, 2013; Viggiani and Casini, 2015; Mandolini and Viggiani, 2017). The subsoil along the Tratta Bassa is characterized by the presence of pyroclastic materials deposited in the area about 12.000 years ago as a result of the volcanic activity of the nearby Phlegrean complex. In particular, the bedrock consists of Neapolitan yellow tuff, a relatively soft volcanic rock characterized by the occurrence of randomly distributed sub-vertical fractures. Above the tuff, there is a layer of uncemented and cohesionless pozzolan, overlaid by another layer of remoulded pozzolan originated by erosion, transport and redeposition processes during the dormant volcanic activity. Later on, a new active phase of the Phlegrean complex deposited at the western part of Tratta Bassa the so-called Neapolitan Pyroclastic Pile, volcanic materials that consists of pumices, ashes and lapilli. Pyroclastic deposits at east are on the contrary overlain by sand of marine origin. Eventually, the area is covered with a more or less thick layer of made ground. Notice that the groundwater table is close to the ground surface. The geological profile along the Tratta Bassa is shown in Figure 5.2:

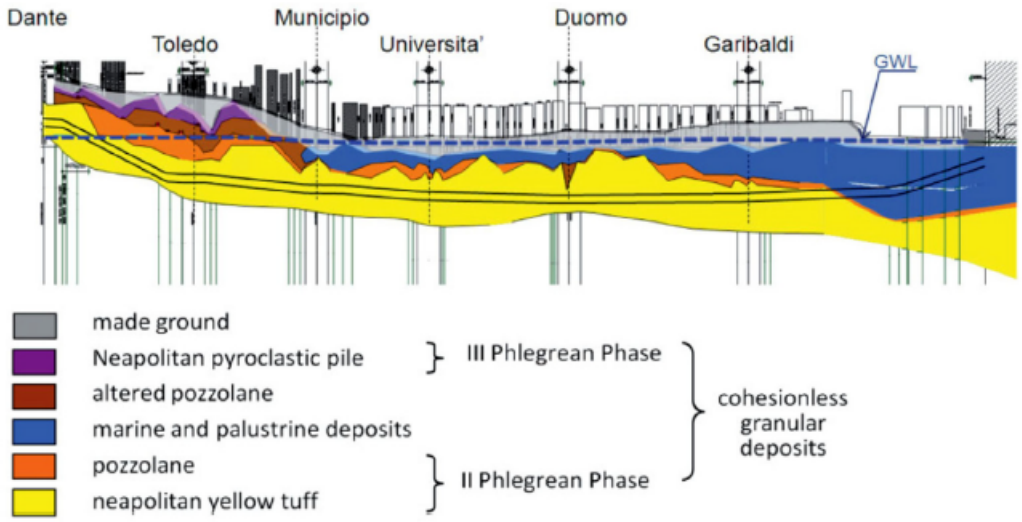

Figure 5.2: Geological profile parallel to the tunnel axis and groundwater conditions along the Tratta Bassa (Viggiani and de Sanctis, 2009)

5.1.2 Design issues

Viggiani (2000) states that in order to minimize the interference with the archaeological findings in the Neapolitan subsoil, tunnels of Line 1 have been excavated within the yellow tuff formation. The significant hydraulic head (25-30 m) together with the occurrence of sub-vertical fractures and the risk of inducing settlements at the surface, have made it necessary the use non-conventional ground improvement methods. In particular, the platform tunnels and some inclined passageways at Municipio, Università, Toledo, Duomo and Garibaldi stations were constructed by means of artificial ground freezing to ensure stability and waterproofing during excavation. The project envisaged the construction of two single-track running tunnels with an outer diameter of 10.48 m, at an average axis-to-axis spacing of 14 m (Lunardi et al., 2007; Russo et al., 2012), as depicted in Figure 5.3:

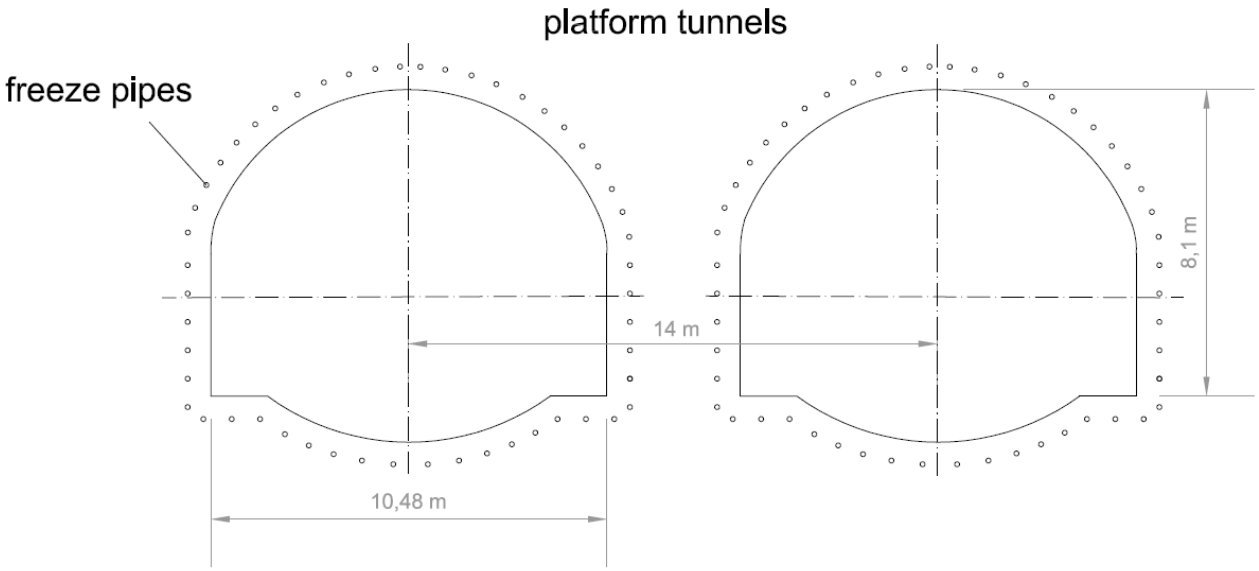

Figure 5.3: Cross section of platform tunnels along Tratta Bassa

More specifically, fifty-two freeze pipes with a diameter of 76 mm, spaced at intervals of 0.75 m, were driven around the future excavation section and alongside the tunnel length for 50 m (Colombo, 2010; Papakonstantinou et al., 2013). Thirty-six of these freeze pipes were installed at the upper part of the tunnel, while the remaining 16 were placed underneath the invert, as illustrated in Figure 5.4. Monitoring of freeze tubes alignment during their installation was fundamental at this stage. By means of the horizontal directional drilling method (HDD) it has been possible to control their orientation and reduce significantly any deviations. However, due to the required length of about 50 m, some misalignments were unavoidable (Russo et al., 2012; Mandolini and Viggiani, 2017). Freezing was activated with liquid nitrogen at about -196°C, and maintained using brine entered at -35°. The mixed method was employed in order to allow a faster and complete formation of the frozen wall, while containing the maintenance costs during excavation. According to project specifications, tunnels construction was undertaken within 1 m thick frozen collar, defined by the contour at -10°C (Mandolini and Viggiani, 2017).

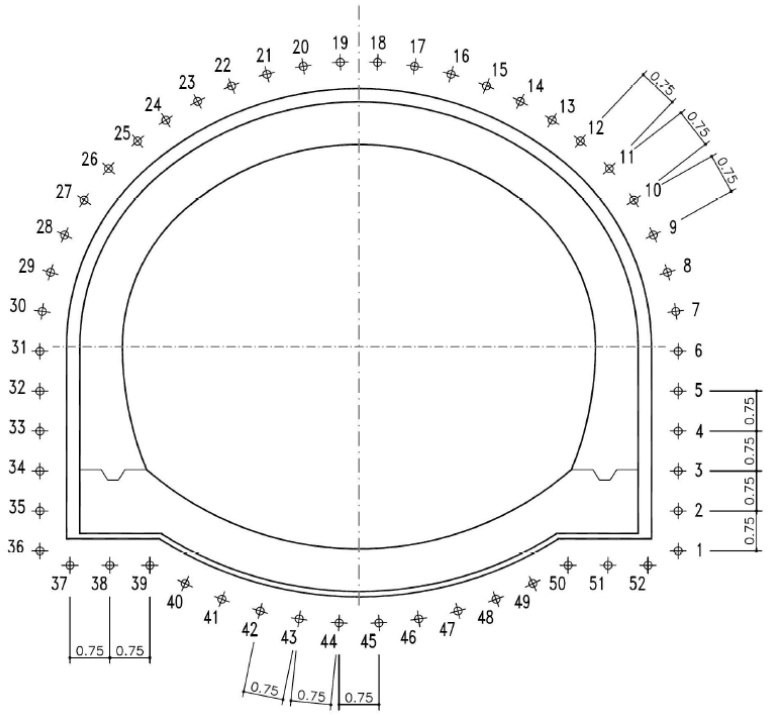

Figure 5.4: Geometry of freeze pipes for a typical platform tunnel of Naples underground metro (Colombo, 2010)

5.1.3 Garibaldi Station

The new underground station in Piazza Garibaldi consists of a 44 m × 22 m rectangular station box to which are connected four single-track tunnels. With a maximum depth of 45 m below the ground level, the station complex is very close to two large residential masonry building, 37 m × 74 m size in plan and consisting of five and seven-story (Mandolini and Viggiani, 2017). A plan view of Garibaldi Station is illustrated in Figure 5.5:

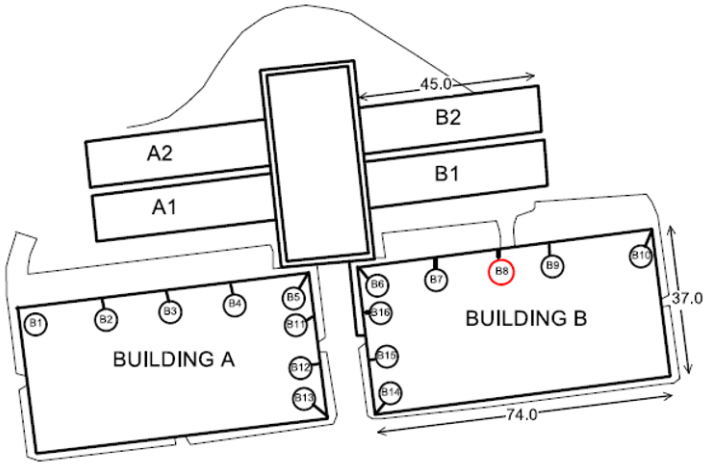

Figure 5.5: Plan view of Garibaldi Station with indication of monitoring points. Particularly interesting is the reference point B8 for which the entire settlement development is available (Mandolini and Viggiani, 2017)

Local ground conditions under Piazza Garibaldi are similar to what it can be found along the whole stretch of Tratta Bassa. The subsoil profile consists of made ground and remoulded ash underlain by alluvial and/or pyroclastic sand over a base of Neapolitan yellow tuff (Viggiani and de Sanctis, 2009; Russo et al., 2012; Papakonstantinou et al., 2010, 2013; Viggiani and Casini, 2015; Mandolini and Viggiani, 2017). Specifically, the pyroclastic sand is also known as pozzolan, namely a fine, loose material containing ash deposits from volcanic falls-out, quite frequent in the Italian geological development. Some geotechnical properties are reported in Figure 5.6:

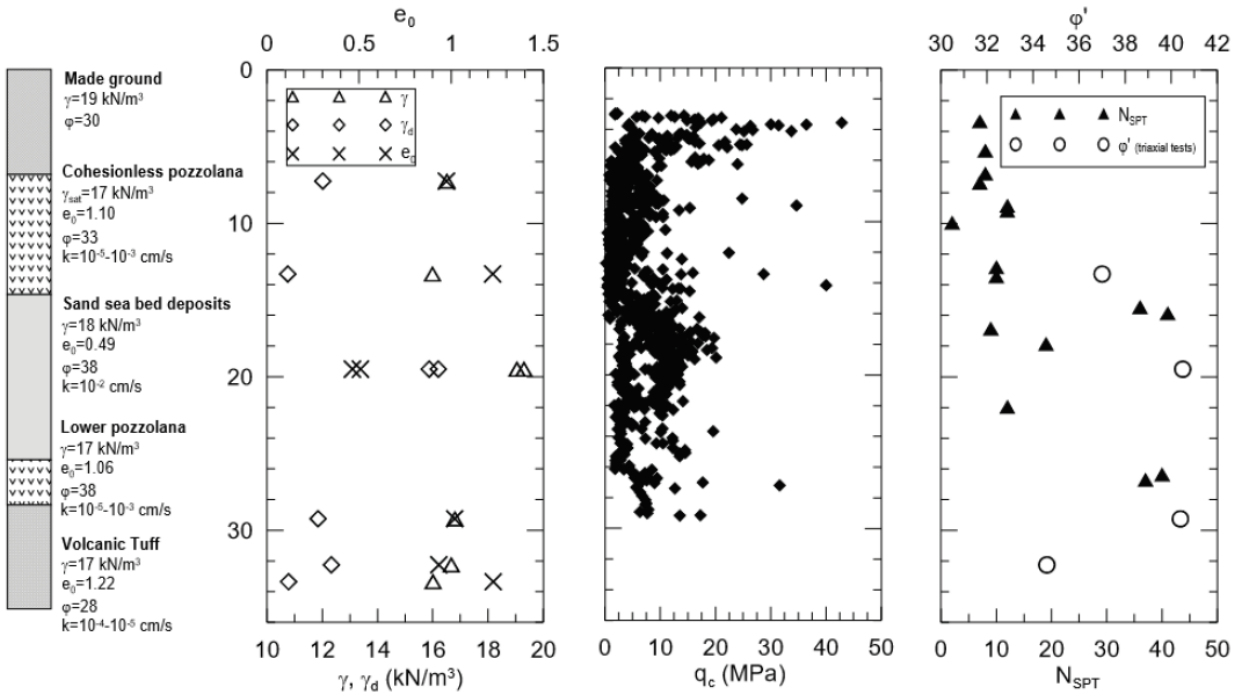

Figure 5.6: Physical and mechanical properties of different layers obtained by laboratory and in-situ investigations at Garibaldi Station (Viggiani and de Sanctis, 2009; Mandolini and Viggiani, 2017)

Even at Garibaldi Station, the crown of the platform tunnels is always contained within the yellow tuff formation and thus well below the groundwater table. The overburden of the tunnel is always about 20 m (Russo et al., 2012) and artificial ground freezing was mainly used here to prevent water ingress into the excavated area from the existing system of sub-vertical fractures of the tuff (Viggiani and de Sanctis, 2009; Mandolini and Viggiani, 2017). In addition, it was possible to retrieve from literature some information concerning construction stages of the platform tunnels at Garibaldi Station (see Table 5.1).

Table 5.1: Construction stages of the tunnel B1 at Garibaldi Station (Viggiani and de Sanctis, 2009)

Construction stage	**Start**	**End**	**Elapsed time**
Freezing	19/10/2004	19/11/2005	387 days
Excavation and lining installation	13/07/2004	19/10/2005	129 days
Thawing	19/10/2005	Total thawing time is unknown	

5.2 Numerical model

A two-dimensional model of the tunnel cross-section has been set up by collecting available information concerning geological stratigraphy of the area, geometry and construction phases of the tunnel, trying to reduce as much as possible uncertainties due to the lack of data. The calculations have been carried out for a generic cross-section of the tunnel B1 at about 30 m away from the station box and closest to the the monitoring reference point B8, for which a complete settlement history at the surface is available for later comparison. Freeze pipes may slightly deviate at this location but the actual pipe alignment is not considered in the numerical model. The reason why it has not been chosen a cross-section closer to the station box is to avoid any influence from the latter, which could make the simulation from a 2D to a 3D problem.

5.2.1 Geometry and boundary conditions

Figure 5.7 shows the computational domain and its spatial discretization. A medium mesh has been used in the calculation to significantly reduce computational times. A line load of 20 kN/m^2 has been applied at the top boundary to simulate the presence on the surface of a seven-story masonry building. Because of symmetry, only the construction of platform tunnel B1 has been modeled (see Figure 5.5 for the plan view and tunnel naming). The local ground conditions at Garibaldi Station have been simplified with respect to the substrata illustrated in Figure 5.6, by assuming only the presence of sand, pozzolan and Neapolitan tuff with the groundwater table at 3,1 m above the ground level. The initial ground temperature was assumed constant with depth and equal to 22°C as it has not been possible to retrieve any data regarding this matter. This value was kept constant at the outer boundaries during the entire process, exception made for the left vertical one representing a symmetry line and hence begin closed for both thermal and water flow. Moreover, groundwater head boundary conditions for were assigned to the bottom and right vertical boundaries. The tunnel was built in AutoCAD and imported into PLAXIS through the Tunnel Designer option. The 52 freeze pipes, which are placed at a distance of about 60 cm around the tunnel opening, have been modeled by defining lines with a length equal to the actual circumference of 238 mm, as depicted in Figure 5.8. Convective boundary conditions were assigned to them, with a transfer coefficient of 10 W/m^2K resulting from trial and error procedure. This type of boundary entails a boundary at which a fluid with a certain temperature transfers heat onto the adjacent material Brinkgreve et al. (2016). The cooling process was modeled by decreasing the temperature to -35°C within a time interval of 10 days, and then keeping it constant during the excavation stage. It was therefore assumed the employment of brine during the whole freezing process, neglecting the activation with liquid nitrogen at -196°C. This is due to the fact that such low temperatures imply zero unfrozen water content, which in turns would have caused numerical issues in the simulation. Then, to simulate the thawing part, an increasing temperature back to 22°C was assigned to the pipes. This should not be intended as a warm fluid circulating within the freeze tubes, but rather as heat propagating from the newly excavated tunnel walls into the ground. This assumption would not have been valid if the distance between the tunnel walls and the freeze pipes had been bigger than it actually is.

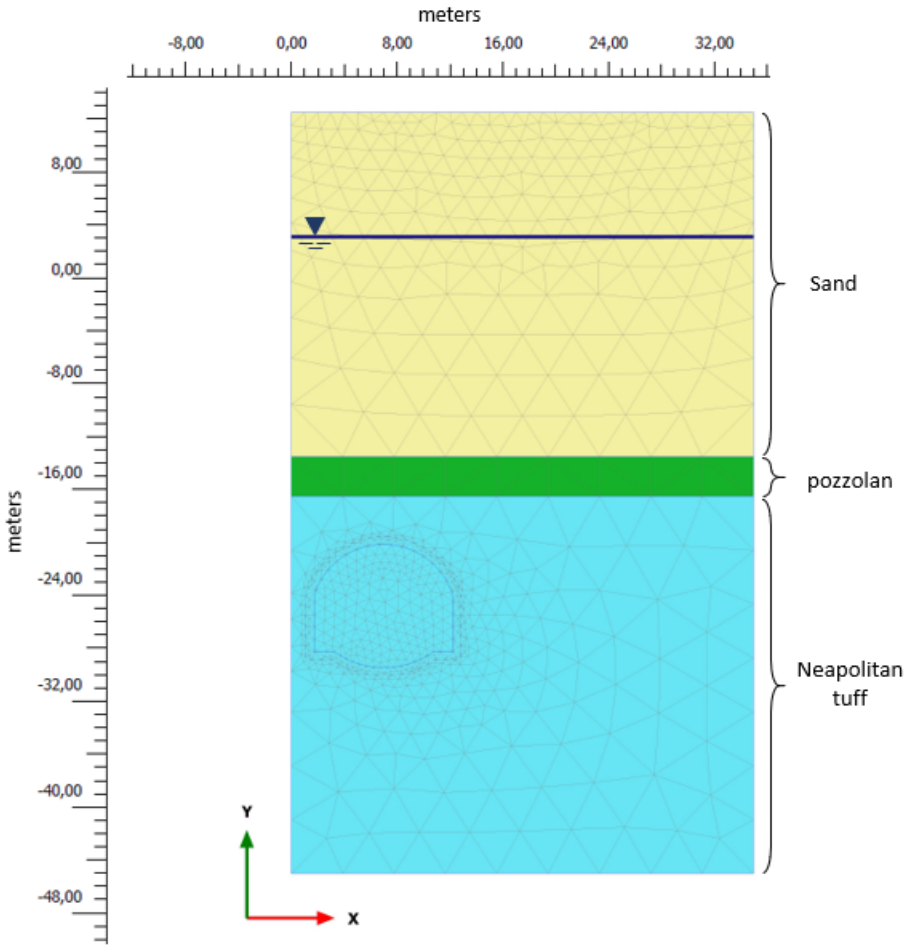

Figure 5.7: Model geometry in PLAXIS

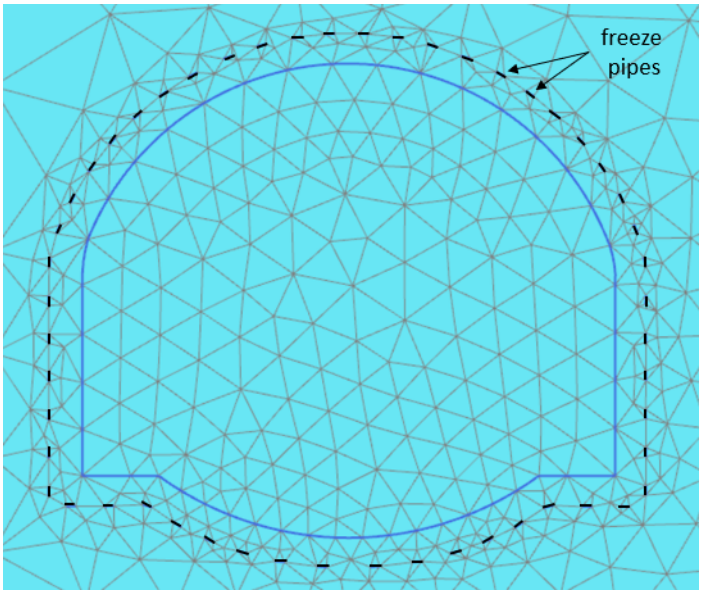

Figure 5.8: Geometry of the modeled freeze pipes around the future tunnel opening

5.2.2 Material data set

The tunnel crown is entirely contained within the yellow tuff, whose material constants have been back-calculated thanks to the previous model calibration and to which one may refer in Chapter 4. Nonetheless, the modification of some parameters was necessary to account for the new model geometry. The adjustments, which specifically refer to the pre-consolidation pressure and its rate of change with depth, are presented in Table 5.2. The ground was assumed homogeneous and the sub-vertical fractures characterizing the tuff were neglected.

Table 5.2: Modified input parameters with respect to the values selected for the model calibration

Parameter	Value
$(p^*_{y0})_{in}$ [N/m^2]	$-350 \cdot 10^3$
Y_{ref} [m]	$-16,5$
Δp^*_{y0} [N/m^2/m]	$-5 \cdot 10^3$

Concerning the other materials, since freezing and thawing do not affect the overlying layers of pozzolan and sand, these two materials were modeled using Hardening Soil (HS) model, rather than the Frozen and Unfrozen Soil model. Material parameters related to both sand and pozzolan were either found in literature or by trial and error (Colombo et al., 2009; Papakonstantinou et al., 2010; Russo et al., 2012; Papakonstantinou et al., 2013; Mandolini and Viggiani, 2017; Fabozzi et al., 2017). Some calculations were required to obtain the specif heat capacity of the pozzolan as only the volumetric heat capacity was provided in literature. Specifically, Eq. 5.1 was used to this purpose (Brinkgreve et al., 2016), where c_v denotes the volumetric heat capacity, n the porosity and S the degree of saturation. The constitutive model parameters used in the simulations are listed in Table 5.3.

$$c_v = (1-n)\rho_s c_s + nS\rho_w c_w \tag{5.1}$$

Table 5.3: Constitutive model parameters for sand and pozzolan

	Parameter	Description	Sand	Pozzolan
General tab sheet	γ_{sat}	Saturated unit weight [N/m^3]	$18 \cdot 10^6$	$16 \cdot 10^6$
	γ_{unsat}	Unsaturated unit weight [N/m^3]	$18 \cdot 10^6$	$16 \cdot 10^6$
	e_0	Initial void ratio [-]	0.49	1.08
Parameter tab sheet	E^{ref}_{50}	Secant stiffness in standard drained triaxial test [N/m^2]	$20 \cdot 10^6$	$47 \cdot 10^6$
	E^{ref}_{oed}	Tangent stiffness for primary oedometer loading [N/m^2]	$20 \cdot 10^6$	$47 \cdot 10^6$
	E^{ur}_{ref}	Unloading/reloading stiffness [N/m^2]	$60 \cdot 10^6$	$95 \cdot 10^6$
	m	Power for stress-level dependency of stiffness [-]	0.5	0.5
	c'_{ref}	Cohesion [N/m^2]	0	0
	ϕ'	Internal friction angle [°]	37	37
Groundwater tab sheet	k_x	Hydraulic conductivity in x-direction [m/s]	$0.01 \cdot 10^{-3}$	$0.6 \cdot 10^{-6}$
	k_x	Hydraulic conductivity in y-direction [m/s]	$0.01 \cdot 10^{-3}$	$0.6 \cdot 10^{-6}$
Thermal tab sheet	c_s	Specific heat capacity [J/(Kg $\cdot$ K)]	860	755
	ρ_s	Density of the solid material [Kg/m^3]	2600	2392
	λ_s	Thermal conductivity [W/m $\cdot$ K]	4.0	0.273

Finally, an elastic plate material was assigned to the tunnel. It was not possible to retrieve any data about the lining properties, but a relative stiff one has been selected by trial and error. The plate element is defined in Table 5.4:

Table 5.4: Lining properties

Axial stiffness - EA	**Flexural rigidity - EI**	**Plate thickness - d**	**Specific weight - w**	**Poisson's ratio - ν**
$14 \cdot 10^9$ N/m	$110 \cdot 10^6$ (N $\cdot$ m^2)/m	0.35 m	6000 N/(m $\cdot$ m)	0.15

5.2.3 Simulation phases

The simulation aims to faithfully reproduce the stages of the real construction process, as briefly described in Table 5.1. A total of 7 phases were created in PLAXIS to model the complete construction of the platform tunnel B1, including freezing and thawing.
In the initial phase, a K_0-procedure generates initial pore pressure and initial effective stresses using the self weight of the modeled soil layers. The subsequent equilibrium phase, created right after the initial phase, serves to guarantee a proper balance of vertical and horizontal stresses within the soil box. It is usually not required by PLAXIS, which tends to deal with this matter in the initial phase, but some numerical improvements were noticed in subsequent calculation steps in this particular simulation. After reaching the equilibrium in the soil box, freezing was activated. It was first assumed that after a period of 10 days, the freezing pipes reached the temperature of -35 °C and then remained constant for another 9 months approximately. This allowed to freeze the surrounding soil and perform the tunnel excavation by deactivating the relative soil cluster. In this very same phase, ground water conditions inside the tunnel was set to dry and the lining was activated. After approximately 4 months of excavation, the temperature of the freeze pipes was raised back to 22°C and then kept constant for 3 months. This was intended to simulate the heat transfer from the tunnel walls into the surrounding ground due to air convection inside the tunnel itself. Figure 5.9 shows the simulated phases in PLAXIS:

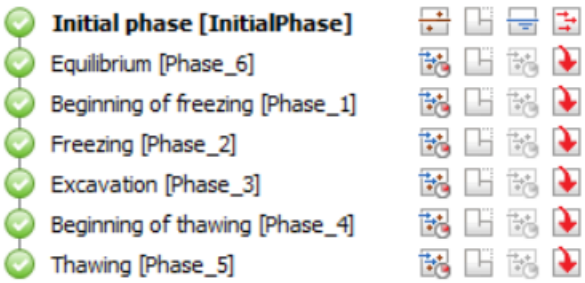

Figure 5.9: Sequence of phases simulated with PLAXIS

All the calculation types were set to fully coupled flow-deformation, except from the initial phase which is characterized by a K0-procedure. Special attention was required to set controlling parameters of the numerical solution during thermal loading. More specifically, the *Max steps* option was set to 10000 for both numerical and flow control parameters, the *Tolerated error* equal to 0.005 for both numerical and flow control parameters and the *Over-relaxation factor*

equal to 0.8 again for both numerical and flow control parameters. Finally, the *Max load fraction per step* option was also changed from default settings and set to 0.1. These suggestions were taken from Ghoreishian Amiri et al. (2016a).

5.3 Results

Simulation results have been plotted in a time-displacement diagram and superposed to the settlement history recorded by the reference point B8 (marked in red in Figure 5.5) during construction works. Results are shown in Figure 5.10:

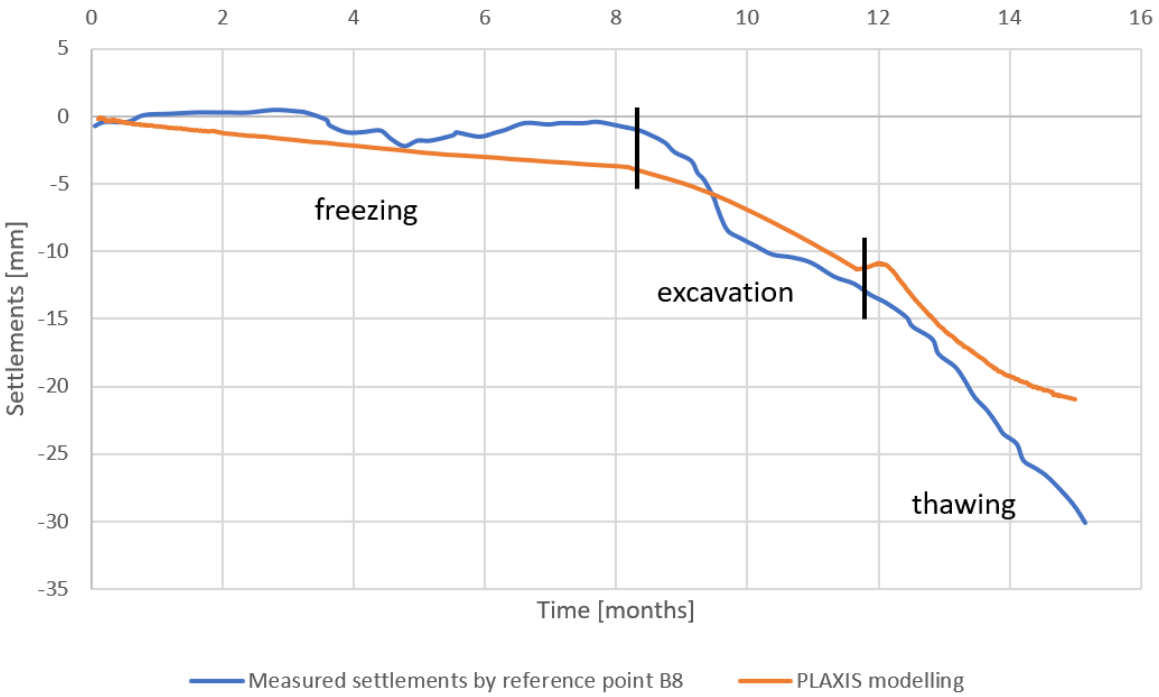

Figure 5.10: Comparison of settlement histories during the entire construction process

As it can be observed from Figure 5.10 above, there is a good agreement between field measurements and simulated results. Despite the significant lack of data and the necessity to make assumptions, the model seems to be robust and able to well predict soil behavior upon freezing and thawing, even when related to large-scale practical applications. Some discrepancies of the PLAXIS modeling from the in-situ settlements measurement can be identified, but a total downward displacement of 21 mm against 30 mm may be however considered a good result. Differences may be especially due to the fact that pipes were assumed and modeled as perfectly aligned to the tunnel opening, while this may not be the case in reality. The formation of a non perfect frozen collar may certainly induce more settlements than what actually expected and predicted by this simulation. Furthermore, there was no information about the exact location of the reference point B8. Despite the attempt to place the nodal point in PLAXIS as close as possible to its real location, inaccuracies of a few meters may have been able to influence the final result. By keeping referring to Figure 5.10, it is possible to observe that half of the set-

tlement occurs during thawing due to the disappearance of the ice and destructuration of the ground which must therefore re-adapt itself to a new equilibrium void ratio (modifications were made to the code in this regard as already described in Chapter 3). The model does not predict any heave on the surface, but this was expected and in accordance with the calibration results. Among the outputs given by PLAXIS, it is possible to inspect the temperature field development during the whole construction process, as depicted in Figures 5.11, 5.12, 5.13 and 5.14:

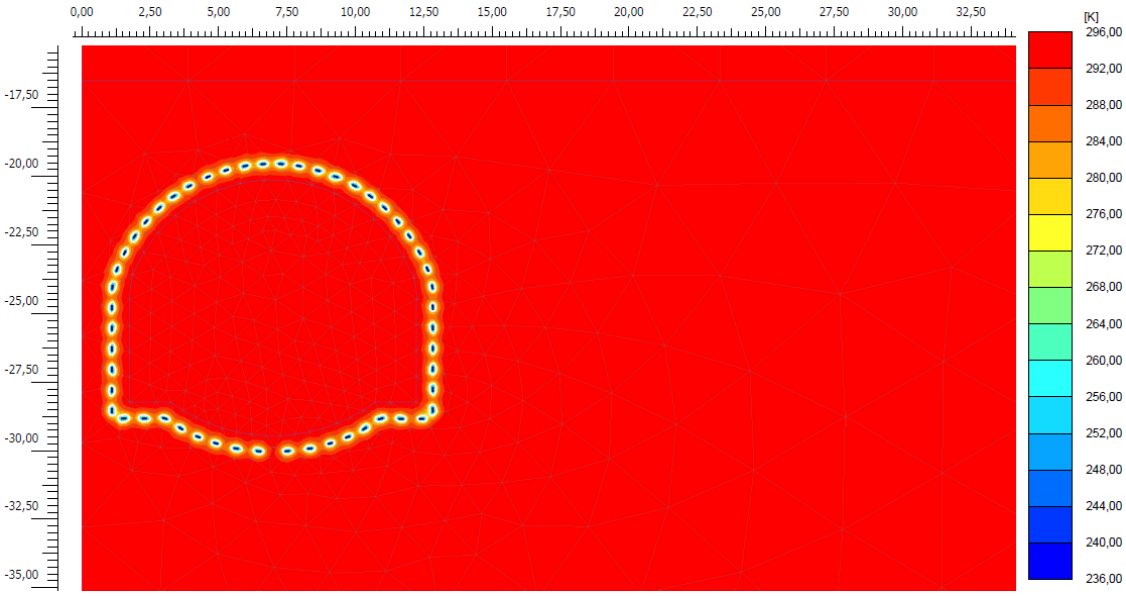

Figure 5.11: Temperature field distribution after 10 days from freezing activation

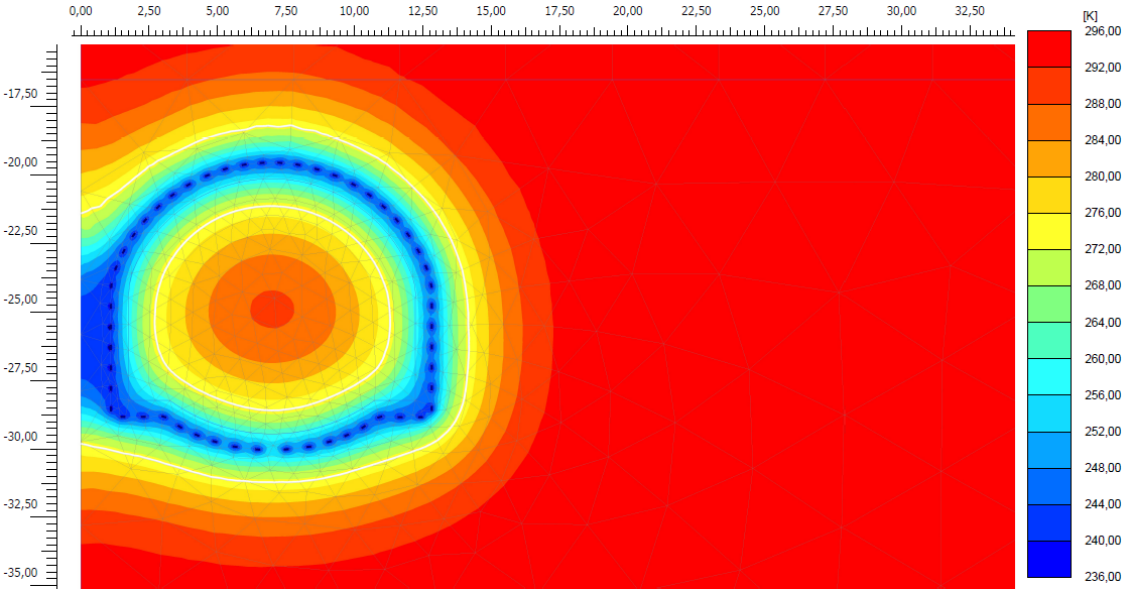

Figure 5.12: Temperature field distribution after approximately 8 months of freezing and before the tunnel is excavated. The white line represents the frost front

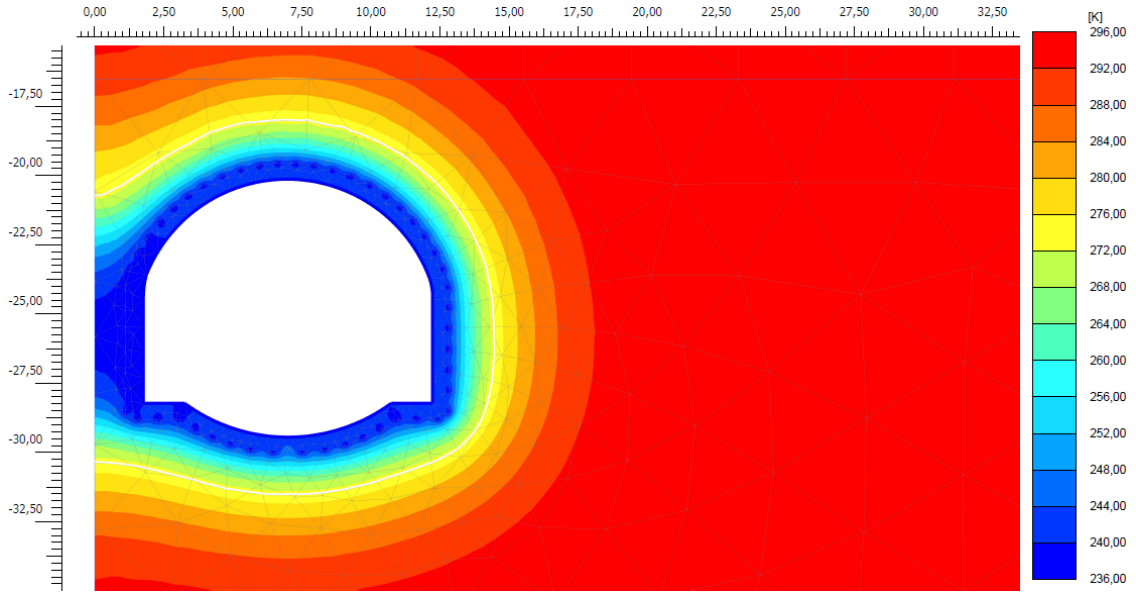

Figure 5.13: Temperature field distribution at the end of the excavation phase

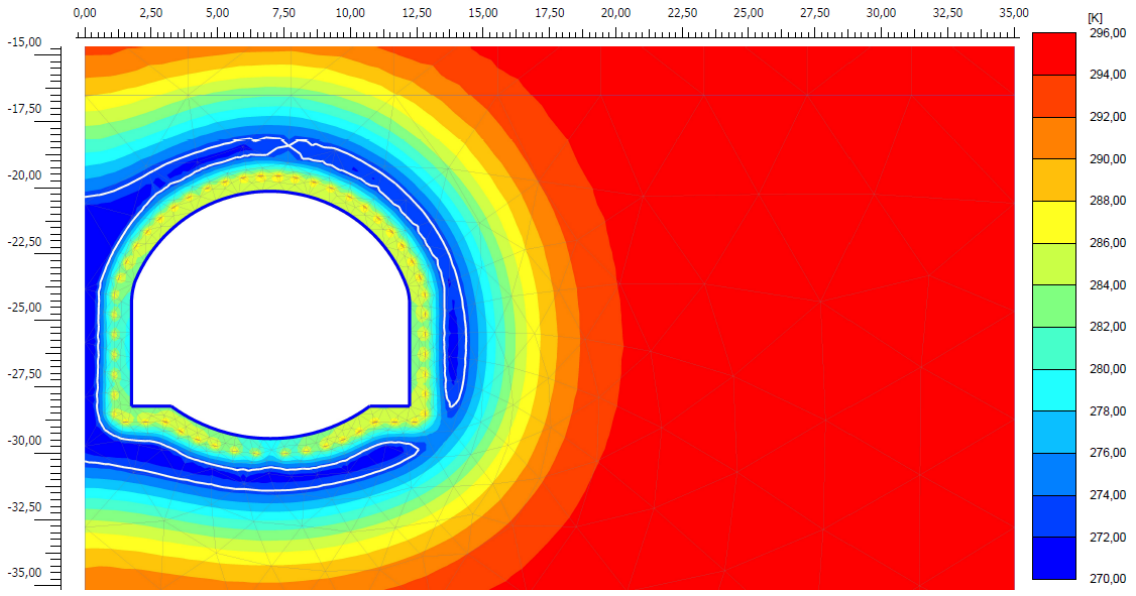

Figure 5.14: Temperature field distribution at the end of the thawing phase: some relatively warm ice is still present around the tunnel opening

Freezing is initiated around the pipes and penetrates through the surrounding ground. The extended low temperature area located next to the left vertical boundary is due to the nearby twin tunnel which was not simulated because of symmetry. The value of the thermal conductivity of the rock, reported in Table 4.1, plays an important role in the frozen wall formation as it controls its thickness development. More specifically, the thickness within the -10°C simulated in the model was found to be approximately equal to 1.3 m, which means nearly 30 cm larger than what envisaged by project details. Despite this difference, this results was considered good enough. Temperature field distribution at the end of the thawing phase is displayed in Figure

5.14. There was, unfortunately, no information concerning the progress of thawing and it was therefore not possible to assess the amount of frozen ground still present after 15 months since the beginning of the construction works. However, the good agreement of the results presented in Figure 5.10 indicates that some ice was still present at this moment, and that the prediction of the model is close to the real case. It is worth noticing in this regard, that the ground temperature has significantly increased and it is nowhere lower than -3°C. This may in turn mean that the thawing process is close to the end. The ice saturation development before and after the excavation, as well as at the end the thawing phase can be found in the Appendix B.

Chapter 6

Discussion and conclusions

The aim of this MSc thesis was to verify and validate the correctness of the theoretical implementation of the new constitutive model and its predictive ability. Roostami (2017) and Aukenthaler (2016) previously performed a similar assessment concluding that the outcome of their simulation was in accordance with the experimental results. Never before, however, was the model successfully applied to a large-scale practical application. Results of this MSc thesis show that there is a very good agreement between numerical simulation results and field measurements from Naples, despite the presence of some minor discrepancies mostly due to the lack of data and the number of simplifying assumptions that had to be made. This final chapter is intended to further analyze the outcome of the simulation performed in this MSc thesis, discussing briefly also the procedure for parameters determination.

6.1 Parameters determination

The crucial part of this MSc thesis is comprised of the calibration of the constitutive model against an oedometer test run on yellow tuff by Pelaéz (2013). Pertinent soil parameters upon freezing and thawing were determined by performing a back-analysis starting from the fact that geometry and deformation behavior were already known. This information, coupled with the numerical modeling, has been the key to correctly estimate soil properties that produced that specific measured behavior. Because of the scarcity of freeze-thaw laboratory tests performed on yellow tuff and to a large number of input parameters, the aforementioned process required quite a long time. Looking at the final results from Garibaldi Station however, the time spent on calibrating the model turned out to be a valuable investment. As a matter of fact, a good calibration often provides the basis for a successful modeling afterward. This MSc thesis provides a good starting parameter set, which if fed into the model, is able to predict quite accurately the frozen and unfrozen behavior of the yellow tuff. It appears clear at this point that a denser laboratory test program will provide more information and an increased certainty about the values of each of those input parameters. As stated also by Ghoreishian Amiri et al. (2016a), isotropic drained compression test and drained simple shear strength test for the unfrozen state of the soil, together with an unconfined triaxial compression test and an isotropic compression test for the frozen state may be indeed used to accomplish this goal. By extending the database con-

taining default parameter sets related to different types of soils and hence the cases in which the Frozen and Unfrozen Soil Model has been successfully applied, means that geotechnical engineers are provided with another powerful tool when dealing with frozen ground.

6.2 Discussion of the results

The most significant result obtained from the numerical modeling is certainly the settlement history at the nodal point close to the reference point B8, which allows to make a comparison with the outcome of the simulation. As already mentioned, nearly half of the settlements occur upon thawing, when the volumetric behavior of the ground is influenced by several competing factors. On one hand, dilative elastic strains will develop due to a negative increment of the cryogenic suction. On the other hand, plastic compressive strains may accumulate as a consequence of the stress level hitting the LC yield surface as a result of structural loss. The latter behavior seems to prevail in this particular simulation case, as no volume increase is experienced. In addition, considering the sampling depth for the oedometer test, the preconsolidation stress of the yellow tuff had to be modified for the simulation of the artificial ground freezing based on the corresponding depth. The change of the preconsiladation stress, which depends on depth and K_0, was found by logical estimation and trial-and-error procedure due to the lack of data. In conclusion, it can be said that the model has been successfully tested even within large practical applications and the simulated frozen soil behavior seems to represent a true picture of the natural behavior.

6.3 Recommendations for future works

Some important topics have not been investigated in this MSc thesis, but that may be done in future. Although it is well known the meaning of each input parameter and their mutual interaction, it remains still somewhat unclear their influence on the yield surface and thus in the overall simulation. A sensitivity analysis should be carried out to facilitate engineers in the selection of parameters, especially when back-analyses is required and a certain degree of uncertainty is present. In future research moreover, equally advanced case studies, as the one presented in this MSc thesis may be investigated by means of the Frozen and Unfrozen Soil Model. Permafrost degradation underneath a road or a runway embankment, slope failure due to an ice-rich cut slope exposure or stresses and deformations related to a buried pipe in Arctic areas could be some examples.

Appendix A

Acronyms

AGF	Artificial Ground Freezing
ARTEK	Arctic Technology Center
ATL	Active Layer Thickness
BVP	Boundary Value Problem
CSL	Critical State Line
DTU	Technical University of Denmark
GS	Grain Segregation
HDD	Horizontal Directional Drilling
HS	Hardening Soil
ITL	Ice Tension Line
LC	Loading Collapse
MCC	Modified Cam Clay
NTNU	Norwegian University of Science and Technology
QTH	Qinghai-Tibet Highway
QTPTL	Qinghai-Tibet Power Transmission Line
THM	Thermo-Hydro-Mehcanical
UDSM	User Defined Soil Model
USCS	Unified Soil Classification System

Appendix B

Modeling of artificial ground freezing

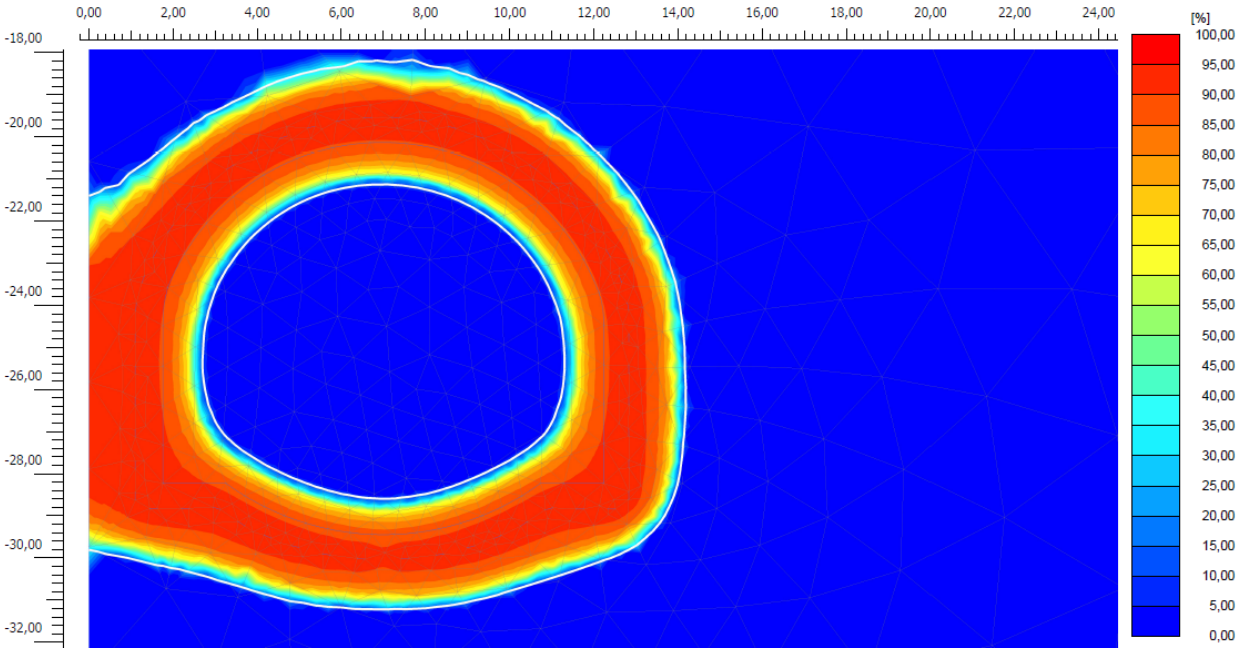

Figure B.1: Ice saturation after approximately 9 months of freezing

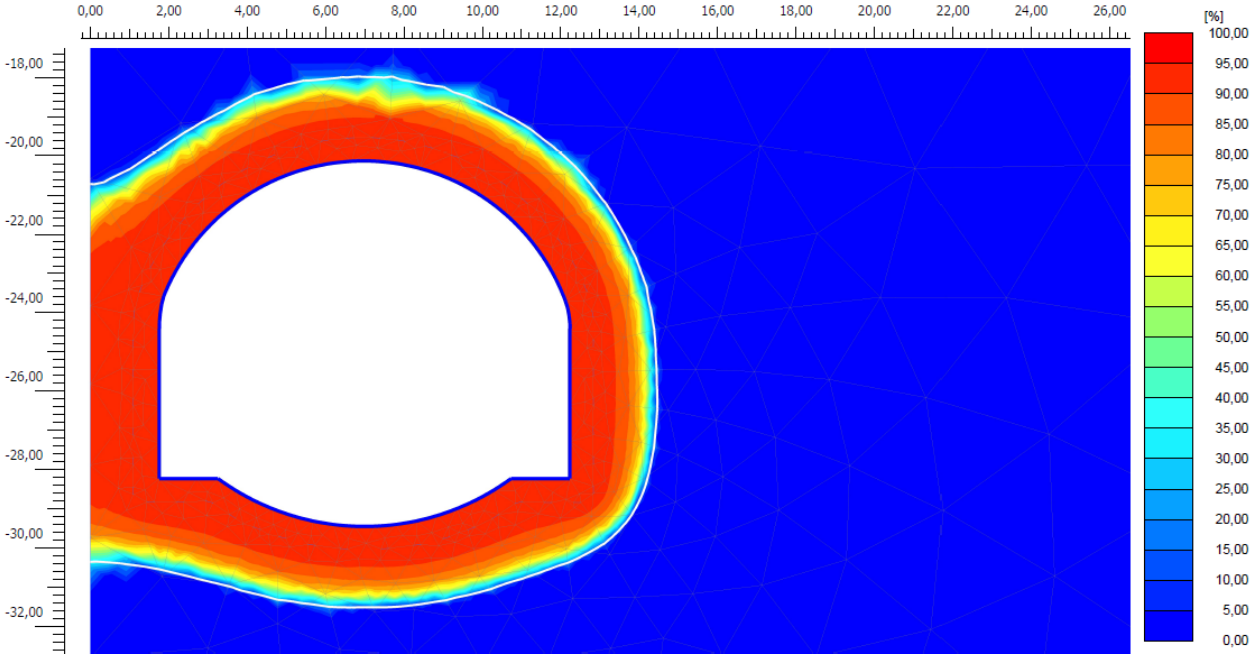

Figure B.2: Ice saturation at the end of the tunnel excavation

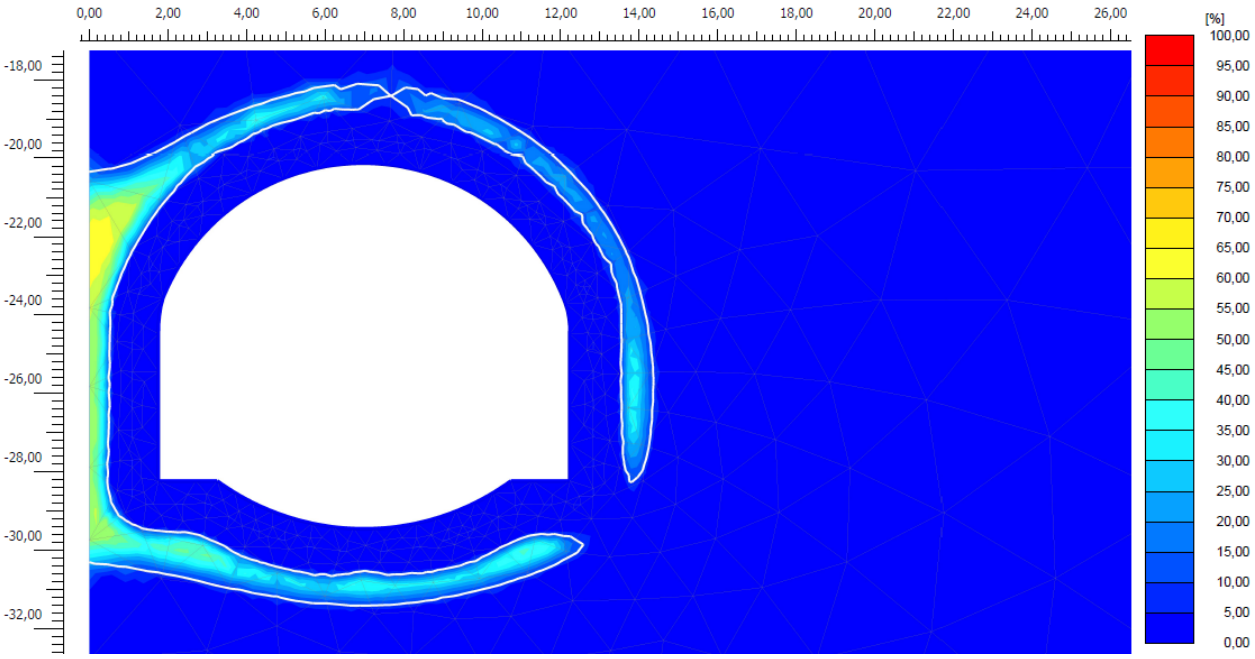

Figure B.3: Ice saturation at the end of the thawing phase

Bibliography

Andersland, O. B. and Ladanyi, B. (2004). *Introduction to Frozen Ground Engineering*. John Wiley and Sons, 2nd edition.

Andersland, O. B., Wiggert, D. C., and Davies, S. H. (1996). Frozen soil subsurface barriers: formation and ice erosion. *Journal of Contaminant Hydrology*, 23:133–147.

Arenson, L. U. and Springman, S. M. (2005). Mathematical descriptions for the bhaviour of ice-rich frozen soils at temperatures close to 0°c. *Canadian Geotechnical Journal*, 42(2):431–442.

Aukenthaler, M. (2016). *The frozen and unfrozen Barcelona Basic Model: a verification and validation of a new constitutive model*. MSc thesis, Delft University of Technology (TU Delft).

Backer, L. and Blindheim, O. (1999). The oslofjord subsea road tunnel: crossing of a weakness zone under high water pressure by freezing. *Challenges for the 21st century. Altan et al. (eds)*.

Baker, T. (1979). Strain-rate effect on the compressive strength of frozen sand. *Engineering Geology*, 13:223– 231.

Benson, C. and Othman, M. (1996). Hydraulic conductivity of compacted clay frozen and thawed in situ. *Journal of Geotechnical Engineering*, 119(2):276–294.

Bourbonnais, J. and Ladanyi, B. (1985a). The mechanical behavior of frozen clay down to cryogenic temperatures. *Proc. 4th Int. Symp. on Ground Freezing*, Sapporo, Japan. Rotterdam: A.A. Balkema, 2:237–44.

Bourbonnais, J. and Ladanyi, B. (1985b). The mechanical behavior of frozen sand down to cryogenic temperatures. *Proc. 4th Int. Symp. on Ground Freezing*, Sapporo, Japan. Rotterdam: A.A. Balkema, 1:235–44.

Brinkgreve, R., Kumarswamy, R., and Swolfs, W. (2016). *PLAXIS manuals*. PLAXIS bv.

Burt, T. and Williams, P. (1976). Hydraulic conductivity in frozen soils. *Earth Surface Processes*, 1(4):349–360.

Christopher, B. R., Schwartz, C., and Boudreau, R. (2006). *Geotechnical Aspects of Pavements*. U.S. Department of Transportation - Federal Highway Administration and National Highway Institute.

Colombo, G. (2010). Il congelamento artificiale del terreno negli scavi della metropolitana di napoli [in italian]. *Rivista Italiana di Geotecnica*, XLIV(4):42–62.

Colombo, G., Lunardi, P., Bruno Cavagna, C., Cassani, G., and Manassero, V. (2009). The artificial ground freezing technique application for the naples underground. *Proceeding of the World Tunnel Congress*, pages 1–15.

Daanen, R. P., Ingeman-Nielsen, T., Marchenko, S., Romanovsky, V. E., Foged, N. N., Stendel, M., Christensen, J. H., and Hornbech Svendsen, K. (2011). Permafrost degradation risk zone assessment using simulation models. *Cryosphere*, 5(4):1043–1056.

Department of the Army (1965). *Soils and Geology: Pavement Design for Frost Condition*. U.S. Government Printing Office.

DiMillio, A. (1995). *A quarter of geotechnical research*. Technical report, Federal Highway Administration. Washington DC, USA.

Eiksund, G., Berggren, A., and Svanø, G. (2001). Stabilisation of a glacifluvial zone in the oslofjord subsea tunnel with ground freezing. *Proceedings of the International Conference on Soil Mechanics and Geotechnical Engineering*, pages 1731–1736.

Fabozzi, S., Licata, V., Autori, S., Bilotta, G., Russo, F., and Silvestri, F. (2017). Prediction of the seismic behavior of an underground railway station and a tunnel in napoli (italy). *Underground Space*, 2:88–105.

Gallavresi, F. (1981). Ground freezing - the application of the mixed method (brine-liquid nitrogen). *Eng.Geol.*, 18:361–375.

GEOFROST (2018). Freezing 120 mbsl in the oslofjord subsea tunnel. `http://www.geofrost.no/article/oslofjordtunnel/`. Accessed on June 5, 2018.

Ghoreishian Amiri, S., Grimstad, G., Aukenthaler, M., Panagoulias, S., Brinkgreve, R., and Haxaire, A. (2016a). *The Frozen and Unfrozen Soil Model*. Technical report - PLAXIS bv 2016.

Ghoreishian Amiri, S., Grimstad, G., Kadivar, M., and Nordal, S. (2016b). Constitutive model for rate-independent behavior of saturated frozen soils. *Canadian Geotechnical Journal*, 53:1646–1657.

Haß, H. and Schäfers, P. (2006). *Application of ground freezing for underground construction in soft ground*. CDM Jessberger GmbH, Bochum, Germany.

Harris, J. S. (1995). *Ground freezing in practice*. Thomas Telford Ltd.

Ingeman-Nielsen, T. (2017). *Lecture notes - 11854 Infrastructure construction in the Arctic*. ARTEK and DTU Byg.

Jones, R. H. (1996). Observation and control of movements in work constructed by ground freezing. In *Geotechnical Aspects of Underground Construction in Soft Ground*, pages 379–384. Mair and Taylor (eds).

Kirkelund, G. M. and Jensen, P. E. (2017). *Lecture notes - 11859 Environmental engineering in the Arctic*. ARTEK and DTU Byg.

Konrad, J. (1989). Effects of freeze-cycles on the freezing characteristics of a clayey silt at various overconsolidation ratios. *Canadian Geotechnical Journal*, 26(2):217–226.

Lackner, R., Amon, A., and Lagger, H. (2005). Artificial ground freezing of fully saturated soil: Thermal problem. *Journal of Engineering Mechanics*, 131(2):211–220.

Ladanyi, B. (1981). Mechanical behaviour of frozen soils. *Proc. Int. Symp. on Mechanical Behaviour of Structures Media*, Volume B, Ottawa:205-245. Carleton Univ: New York: Elsevier.

Lai, Y., Yang, Y., Chang, X., and Li, S. (2010). Strength criterion and elastoplastic constitutive model of frozen silt in generalized plastic mechanics. *International Journal of Plasticity*, 26(10):1461–1484.

L'Amante, D., Flora, A., Russo, G., and Viggiani, C. (2012). Displacement induced by the installation of diaphragm panels. *Acta Geotechnica*, 7:203–2018.

Lunardi, P., Cassani, G., and De Giudici, C. (2007). Design and executive aspects of the construction of the line 1 of the naples metro. *Proceedings of the International Symposium on Tunnelling for Urban Development*.

Mandolini, A. and Viggiani, G. (2017). Experiences gathered from the construction of napoli undergound. *Procedia Engineering*, 172:31–41.

Max Bögl Group (2018). Infrastructure ground freezing technology. `https://www.max-boegl.de/en/downloads-en/55-infrastructure-ground-freezing-technology/file.html`. Accessed on April 5, 2018.

Mu, Y., Li, G., Ma, W., Wang, D., and Wang, F. (2016a). Numerical study of long-term cooling effects of thermosyphons around tower footings in permafrost regions along the qinghai-tibet power transmission line. *Cold Regions Science and Technology*, 121:237–249.

Mu, Y., Li, G., Yu, Q., Ma, W., Wang, D., and Wang, F. (2016b). Numerical study of long-term cooling effects of thermosyphons around tower footings in permafrost regions along the qinghai-tibet power transmission line. *Cold Regions Science and Technology*, 121:237–249.

National Snow and Ice Data Center (2018). All about frozen ground. `https://nsidc.org/cryosphere/frozenground/index.html`. Accessed on January 18, 2018.

Nelson, F. E., Anisimov, O. A., and Shiklomanov, N. I. (2001). Subsidence risk from thawing permafrost: the threat to man-made structures across regions in the far north can be monitored. *Nature*, 410(6831):889–890.

Nishimura, S., Gens, A., Olivella, S., and Jardine, R. (2009). Thm-coupled finite element analysis of frozen soil: formulation and application. *Géotechnique*, 59:159–171.

Pan, Y. and Wu, C. (2002). Numerical investigations and engineering applications on freezing expansion of soil restrained two-phase closed thermosyphons. *Int. J. Therm. Sci.*, 41:341–347.

Papakonstantinou, S., Agnastou, G., and Piementel, E. (2010). Analysis of artificial ground freezing in the pari-duomo platform tunnel of the naples metro. In *Numerical Methods in Geotechnical Engineering*, pages 3–8. CRC Press. doi:10.1201/b10551-3.

Papakonstantinou, S., Agnastou, G., and Piementel, E. (2013). Evaluation of ground freezing data from the naples subway. *Geotechnical Engineering*, 166:280–298.

Pelaéz, R. (2013). *Congelación artificial de los suelos naturales. Un enfoque experimental con desarrollo de equipo.* [in Spanish] MSc thesis at Politechnical University of Catalonia (UPC).

Rempel, A., Wettlaufer, J., and Grae Worster, M. (2004). Premelting dynamics in a continuum model of frost heave. *J. Fluid Mech.*, 498:227–244.

Rocca, O. (2011). *Congelamento artificiale del terreno.* [In italian]. Napoli: Hevelius Edizioni.

Romanovsky, V. E., Smith, S. L., Isaksen, K., Shiklomanov, N. I., Streletskiy, D. A., Kholodov, A. L., Christiansen, H. H., Drozdov, D. S., G. V. Malkova, G., and Marchenko, S. S. (2017). Terrestrial permafrost [in arctic report card 2017].

Roostami, H. (2017). *Finite element analysis of couples thermo-hydro-mechanical processes in fully saturated, partially frozen soil.* MSc thesis, Norwegian University of Science and Technology (NTNU).

Russo, G., Viggiani, C., and G.M.B., V. (2012). Geotechnical design and construction issues for lines 1 and 6 of the naples underground. *Geomechanics and Tunnelling 5*, 3:300–311.

Sayles, F. H. and Carbee, D. L. (1981). Strength of frozen silt as a function of ice content and dry unit weight. *Engineering Geology*, 18:55–66.

Sinitsyn, A. O. and Løset, S. (2011). Strength of frozen saline silt under triaxial compression with high strain rate. *Soil Mechanics and Foundation Engineering*, 48(5):196–202.

Smith, N. (2012). *Artificial ground freezing.* In: Temporary Works: Principles of Design and Construction, Grant M. and Pallet F.P., (eds). London, United Kingdom: ICE Publishing, p. 109-116.

Solomon, S., Qin, D., Manning, M., Chen, Z., Marquis, M., Averyt, K., Tignor, M., and Miller, H. (2007). *IPCC, 2007: Contribution of Working Group I to the Fourth Assessment Report of the Intergovernmental Panel on Climate Change.* Cambridge, UK and New York, NY, USA. Cambridge University Press.

Spaans, E. and Baker, J. (1996). The soil freezing characteristic: its measurement and similarity to the soil moisture characteristic. *Soil Science Society of America Journal*, 60(1):13–19.

Stoss, K. and Valk, J. (1979). Uses and limitations of ground freezing with liquid nitrogen. *Eng. Geol.*, 13:485–494.

Streletskiy, D. A., Shiklomanov, N. I., and Nelson, F. E. (2012). Permafrost, infrastructure and climate change: a gis-based landscape approach to geotechnical modeling. *Arctic, Antarctic, and Alpine Research*, 44(3):368–380.

Thomas, H., Cleall, P., Li, Y.-C., Harris, C., and Kern-Luetschg, M. (2009). Modelling of cryogenic processes in permafrost and seasonally frozen soils. *Géotechnique*, 59(3):173–184.

Tice, A., Anderson, D., and Banin, A. (1976). The prediction of unfrozen water contents in frozen soils from liquid limit determination. *US Army Cold Regions Research and Engineering, Laboratory Report CRREL 76-8*.

Ting, J., Martin, R., and Ladd, C. (1983). Mechanisms of strength for frozen sand. *ASCE J Geotech Eng*, 109(10):1286–1302.

Trevi S.p.a. (2013). Artificial ground freezing - technology. `http://www.trevispa.com/downloads/2943/1486/GroundFreezing2013.pdf`. Accessed on January 11, 2018.

Van Dorst, A. (2013). *Artificial ground freezing as a construction method for underground spaces in densely built up areas*. MSc thesis, TU Delft.

Viggiani, C. (2000). Aspetti geotecnici e scelte di progetto [in italian]. *La Metropolitana di Napoli - nuovi spazi per la mobilità e per la cultura*, pages 145–153.

Viggiani, G. and Casini, F. (2015). Artificial ground freezing: from applications and case studies to fundamental research. *XVI European Conference on Soil Mechanics and Geotechnical Engineering*.

Viggiani, G. and de Sanctis, L. (2009). Geotechnical aspects of underground railwa construction in the urban environment: the examples of rome and naples. *Geological Society, London. Engineering Geology Special Publication*, 22:215–240.

Wettlaufer, J. and Grae Worster, M. (2006). Premelting dynamics. *Annual Review of Fluid Mechanics*, 38(1):427–452.

Yuanming, L., Yugui, Y., C., X., and L., S. (2010). Strength criterion and elastoplastic constitutive model of frozen silt in generalized plastic mechanics. *International Journal of Plasticity*, 26:1461–1484.